ASSESSMENT OF THE ITER HIGH-FREQUENCY MAGNETIC DIAGNOSTIC SET

presented by D.Testa on behalf of

H.Carfantan[2], R.Chavan, Y.Fournier[3], J.Guterl, J.B.Lister, T.Maeder[4], J-M.Moret, A.Perez, F.Sanchez, B.Schaller[3], C.Slater[3], M.Stoeck[3], M.Toussaint and G.Tonetti

Centre de Recherches en Physique des Plasmas, Ecole Polytechnique Fédérale de Lausanne, Association EURATOM-Confédération Suisse, CH-1015 Lausanne, Switzerland

[2]LATT, Université de Toulouse - CNRS, 31400 Toulouse, France

[3]Laboratoire de Production Microtechnique (LPM), EPFL, CH-1015 Lausanne, Switzerland

e-mail address of contact author: duccio.testa@epfl.ch

OUTLINE

the ITER HF magnetic diagnostic system:

- the measurement requirements
- the baseline system design
- the tools for the system optimization analysis
- testing the measurement performance of the ITER nominal diagnostic layout and different alternative (non-)optimized variants
- the proposal for an “optimized” system design
- summary and conclusions

REFERENCES and FURTHER INFO

- ITER measurement requirements: G.VAYAKIS et al., Rev. Sci. Instrum. **74** (2003), 2409; A.J.H.DONNÉ et al., "Chapter 7: Diagnostics", in "Progress in the ITER Physics Basis", Special Issue of Nucl. Fusion **47** (2007); the original description of the ITER measurement requirements for the HF magnetic diagnostic system are presented in Table-2 in the Design Description Document DDD 5.5.A, ITER document reference "N55DDD101-06-12W0.3"; see also the presentations made at the ITER diagnostic review meeting on 9-13 July 2007
- measurement requirements for HF instabilities in ITER as recommended by ITPA MHD and EP working groups: see ITPA webpages
- D.Testa et al., *The magnetic diagnostic set for ITER*, IEEE Transactions on Plasma Science **38**(3) (2010), 284-294
- D.Testa et al., *Functional performance analysis and optimization for the high-frequency magnetic diagnostic system in ITER*, Fusion Science and Technology **57**(3) (2010), 208-273
- D.Testa et al., *Prototyping a high frequency inductive magnetic sensor using the non-conventional, low temperature co-fired ceramics technology for use in ITER*, accepted for publication in Fusion Science and Technology, August 2010
- D.Testa et al., *Prototyping the ITER high frequency magnetic sensor using the conventional, Mirnov-type, pick-up coil*, submitted for publication to Fusion Science and Technology, 2009
- D.Testa et al., *Baseline System Design and Prototyping for the ITER High-frequency Magnetic Diagnostics Set*, Proceedings SOFE 2009 Conference
- **M.Toussaint et al., *Design of the ITER High-Frequency Magnetic Diagnostic Coils*, this SOFT 2010 Conference**

Challenges for the Measurement and the MHD Analysis in ITER

- **multiple degenerate modes** expected at nearly the same frequencies
- **need precise ±1 determination** of toroidal and poloidal mode numbers for active feedback control and MHD spectroscopy in real-time
- **real-time applications** require <1ms clock-rate
- **uneven spatial sampling must be applied**
  - spatial Nyquist numbers cannot be achieved due to installation constraints
- **must conserve phase relation between I/Q components of measured fluctuation spectrum**
  - stable vs. unstable instabilities, damping and growth rate
- **blind analysis**, no previous knowledge of fluctuation spectra can be used
- **situation further complicated by the need for redundancy and resilience to the loss of sensors**
  - no easy access to inside of the vessel to replace faulty sensors
  - therefore "*risk management plan*" over the entire life of ITER (>30 years)

Measurement Requirements for MHD Instabilities: the ITER view

main ITER measurement requirements: detect modes with $|n| \leq 50$, $q=m/n=2$, $|\delta B_{MEAS}/\delta B_{POL}| \sim 10^{-4} \sim 1G$

measurement	parameter	condition	range	ΔT or ΔF	ΔX or Δk	2σ accuracy
high-frequency MHD macro instabilities: fishbones, AEs, ACs, EPMs, ELMs, RWMs, NTMs, sawteeth and disruption precursors	global AEs, fishbones: fluctuations in [B, T, n]	all ITER scenarios	$I_p \geq 15MA$ $B_\phi \geq 6T$	0.1-10kHz *≤100kHz*	(m,n)=(1,1) *(|m|,|n|)=(5,3)*	±30% *n,m: ±0* *$\|\delta B_{MEAS}\|$: ±15%*
	sawteeth, ELMs and disruption precursors	all ITER scenarios	$I_p \geq 15MA$ $B_\phi \geq 6T$	0.1-10kHz *≤100kHz*	(m,n)=(1,1) *(|m|,|n|)=(5,3)*	±30% *n,m: ±0* *$\|\delta B_{MEAS}\|$: ±15%*
	high-n/m AE-driven fluctuations in [B, T, n]	all ITER scenarios	$I_p \geq 15MA$ $B_\phi \geq 6T$	up to 2MHz *≤1MHz*	n=10–50 *|n|=5–30* *|m|=10–60*	±30% *n,m: ±1 to ±3* *$\|\delta B_{MEAS}\|$: ±30%*

list of the ITER measurement requirements relevant to the in-vessel HF sensors
in red italic the requirements that have been used in this work (ITPA-MHD/EP work)

Measurement Requirements for MHD Instabilities in ITER – ITPA logic

- ITER "nominal" measurement requirements: detect single modes with $|n|\leq 50$, $|m|\leq 100$ (use q~2 as for NTMs), $|\delta B_{MEAS}/\delta B_{POL}|\sim 10^{-4}$ (hence **$|\delta B_{MEAS}|\sim 1G$**), sensor's effective area $0.03<(NA)_{EFF}[m^2]<0.1$, frequency range $\leq$2MHz
- current measurement capabilities on existing devices (JET, ASDEX-U, DIII-D, JT-60U, MAST): **$|\delta B_{MEAS}|\sim mG$**, $|n|\sim|m|\sim 20$, $(NA)_{EFF}\sim 0.05m^2$, frequency range $\leq$2MHz
- predictions for HF instabilities in burning plasma regimes in ITER: **multiple** (n,m) modes co-existing, most dangerous modes with n~5-20 and q~2 with expected growth rate **$\gamma/\omega>0.001$**, frequency range up to ~1MHz, stochasticity threshold for α's radial transport $|\delta B_{MEAS}/\delta B_{POL}|\sim 10^{-4}$ (hence **$|\delta B_{MEAS}|\sim 1G$ as in ITER requirements**)
- *conclusions: problems with nominal ITER measurement specifications:*
  - **the required $|\delta B_{MEAS}/\delta B_{POL}|\sim 10^{-4}$ is too close to the stochasticity limit for radial transport of αs ➔ need to detect 10-100 smaller $|\delta B_{MEAS}|\sim mG$ as expected from predicted growth rates $\gamma/\omega\sim 0.001$**
  - **multiple frequency-degenerate modes predicted to occur**
  - **$|m|\geq 2|n|$ need to be correctly detected**
  - acceptable error on $|\delta B_{MEAS}|$ ➔ $\pm$15%
  - acceptable error on (n,m) ➔ $\pm$0 for $(|n|,|m|)<5$ (real-time), $\pm$1 for $6\leq(|n|,|m|)\leq 15$ (main fast ion physics), $\pm$(2-3) for $(|n|,|m|)>20$ (turbulence)

New Regimes for AE Interaction with α's Expected for Q>5

test simulation: single n=6/m=10 mode interacting with α's (in ITER)

need for real-time detection of dangerous MHD modes for active feedback control
➔ *real-time control details depends on specific (n,m)*

test simulation: **multiple n=5-10** modes interacting with α's (in ITER): **$|\delta B_{MEAS}|$~1G!!**

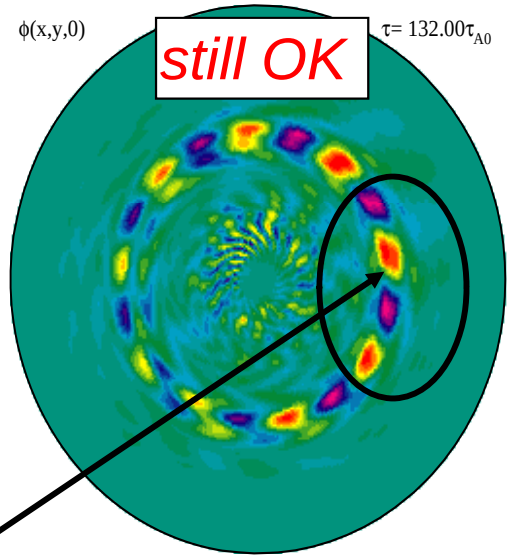

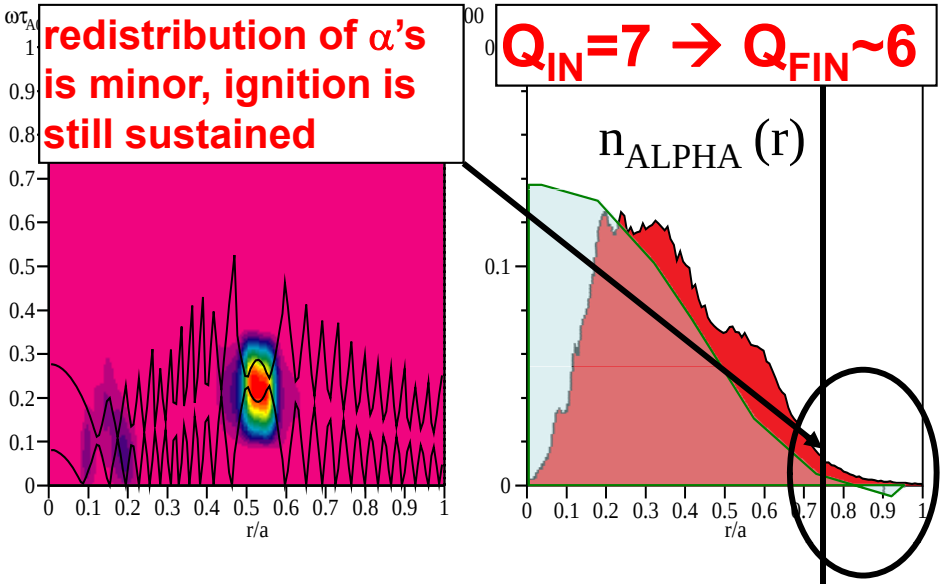

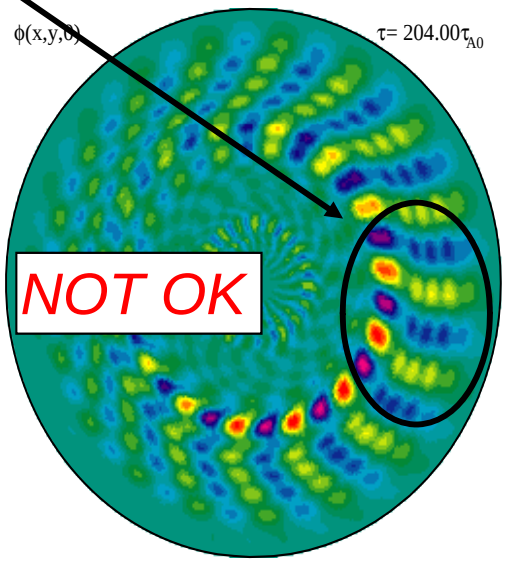

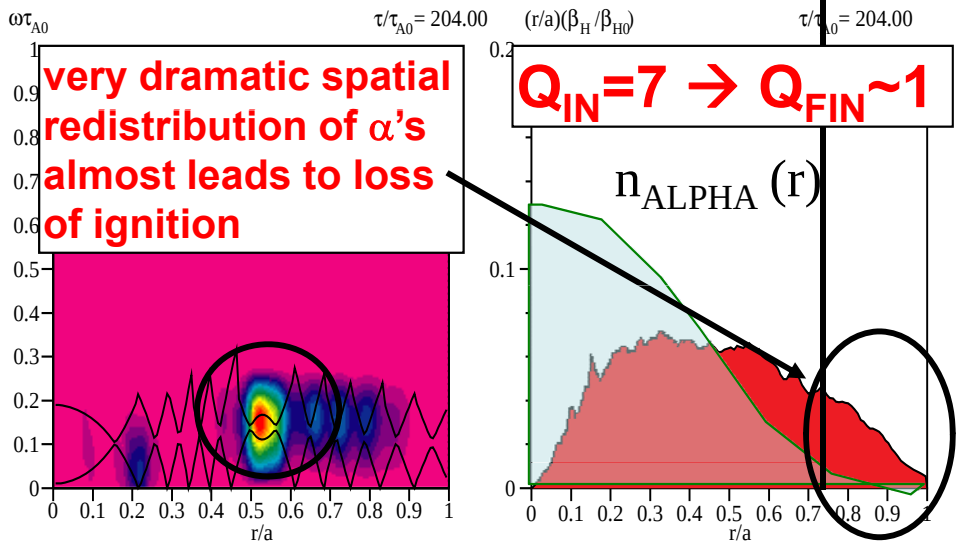

Active MHD Spectroscopy for Plasma Diagnostic Needs Precise Determination of Frequency-Degenerate Mode Numbers

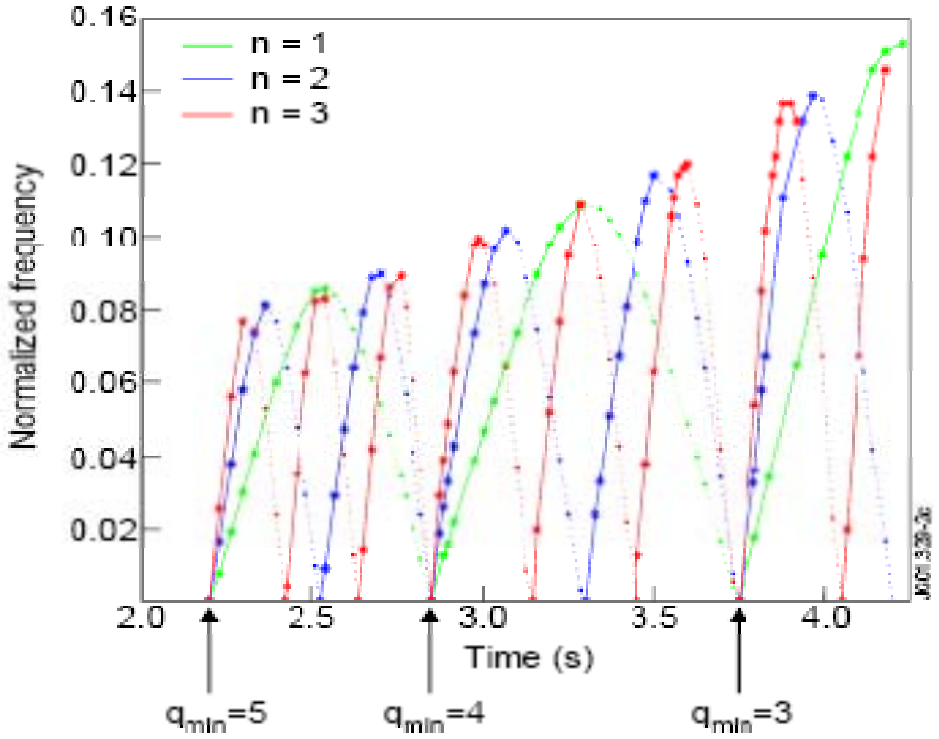

Time evolution n=1, n=2, and n=3 continuum tips during $q_{min}(t)$ evolution

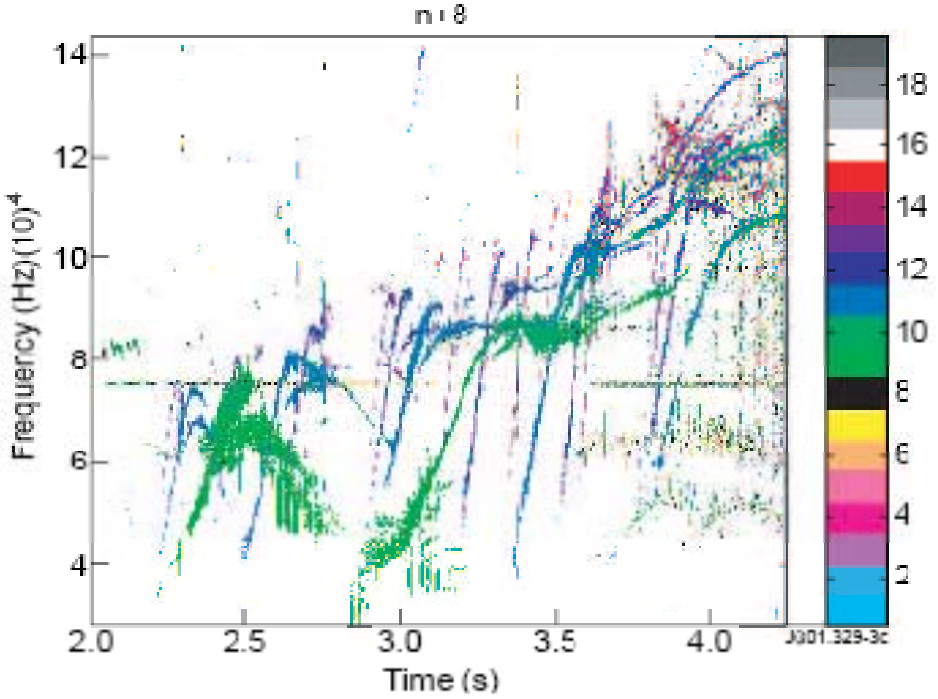

Magnetic spectrogram showing Alfven Cascade Eigenmodes in reversed-shear JET plasma (pulse #49382)

Alfvén Cascades are routinely used in JET/DIII-D/JT-60U for diagnosing current profile evolution

➔**potential for real time application in ITER: improvements of τ_E, confinement of α's!**

➔**detection of multiple concurrent (n,m) components is required**

Must Use an Universal System Optimization Strategy

- **tests on sensitivity to noise in the measurements** ➔ can random noise be mistaken for real modes?
- **tests on false alarms** ➔ modes that are not in the input spectrum but that will trigger a control reaction to save the plasma if they are wrongly detected
- **tests on importance of missing sensors** ➔ resilience of the measurement performance against the loss of faulty sensors
- **tests on installation, measurement and calibration errors leading to an apparent shift in the position of the sensors** ➔ how sensitive is the measurement performance of the selected geometry against such errors?
- measurement requirements define correct and wrong detection of the modes
- **must normalize measurement performance wrt to R&D and installation costs to account for the number of sensors**
- **all these tests are performed by optimizing the spectral window using a minimization of its maxima for integer mode numbers**
  - we measure the periodogram: the convolution of the input mode spectrum with the spectral window determined by the sensors' positions

Why do we Need to Optimize the Measurement Spectral Window?

- toroidal periodogram: convolution of the input mode spectrum with the **Spectral Window $W(n) = \Sigma_k \exp(i2\pi\phi_k n)$** related to the sensors' positions ϕ_k
- an example using JET simulated data:

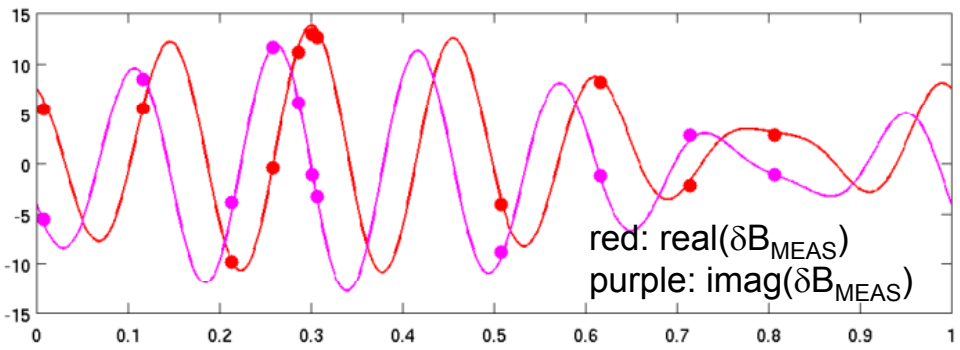

input data mapped onto the full set of 11 HF **non-optimized** magnetic sensors

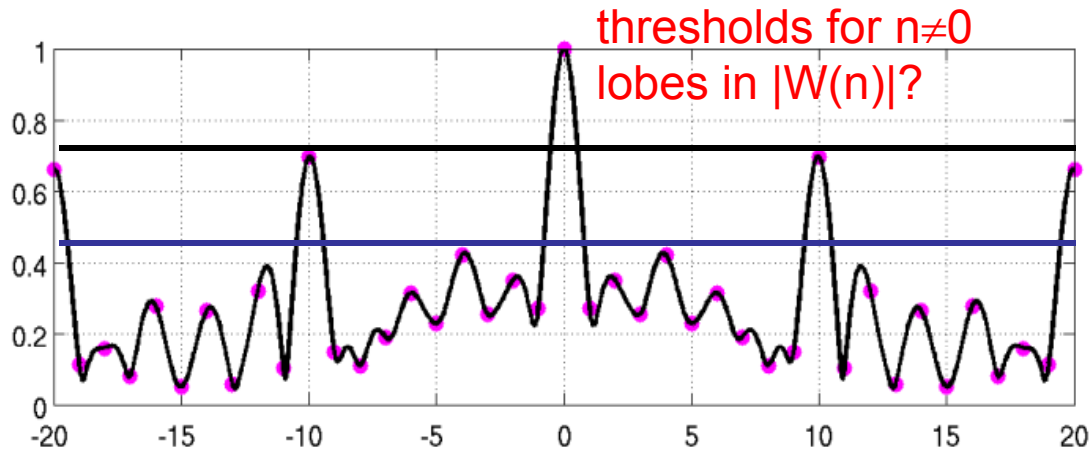

spectral window |W(n)|: high n≠0 secondary lobes underlying regularity of sensors' position

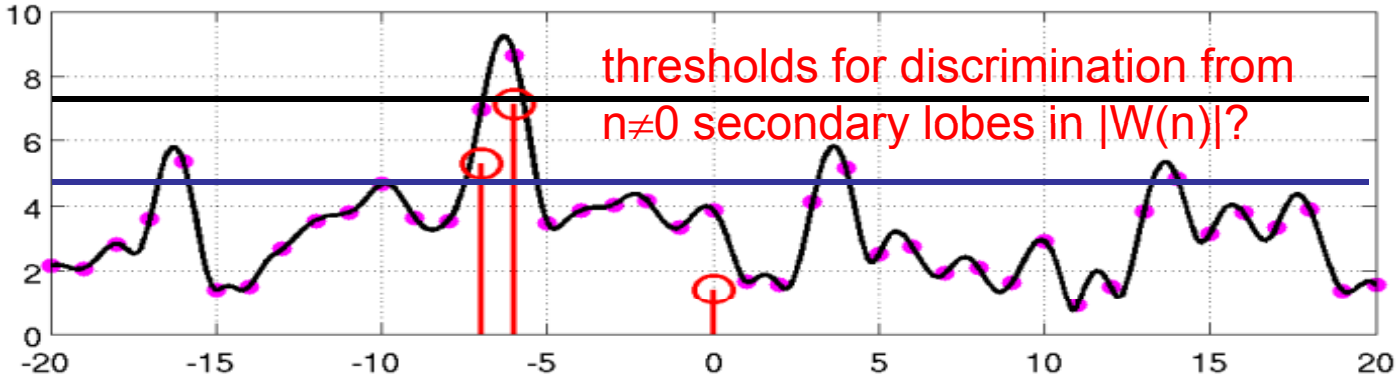

periodogram: the red circles are the input modes, how to discriminate reliably between all possible solutions (purple dots) obtained with a non-optimized sensors' geometry?

Analysis Methods from Astronomy and Astrophysics to Fusion Plasmas

- **from JET to ITER: we need to find an algorithm for a reliable optimization of the spectral window**
- finding periodic waveforms in un-evenly sampled data is an ubiquitous problem in the field of astronomy
  - temporal frequencies in astronomical data correspond to spatial mode numbers in fusion plasmas
  - un-evenly sampled data in un-bounded time domain are the analog of data from un-evenly distributed Mirnov sensors in bounded toroidal and poloidal angle coordinates
- however there are some differences:
  - in astronomy: real valued data and real valued frequencies
  - in tokamaks: complex valued data and integer mode numbers (periodic boundaries ≡ integer frequencies in A&A)
- a new method for fitting sinusoids to irregularly sampled data considering explicitly high $n \neq 0$ secondary lobes in the spectral window has been recently proposed, based on the principle of the **Sparse Representation of Signals**: the **SparSpec** code
  - freely available at: http://www.ast.obs-mip.fr/Softwares

the Sparse Representation Method

SparSpec minimizes the L1-norm penalized criterion:

$$J(x) = \tfrac{1}{2}\left\|\mathbf{y} - W\mathbf{x}\right\|^2 + \lambda \sum_{k=-K}^{K} \left|x_k\right|_{L1}$$

y: vector of data taken at time t_k [≡ position ϕ_k]
W: spectral window $\exp(i2\pi t_k f_n)$ [≡ $\exp(i2\pi\phi_k n)$]
x: vector of (I,Q) signals for frequencies f_n
λ: parameter fixed to obtain a satisfactory sparse solution ➔ **penalty criterion for invoking more modes to find adequate solution**
λ can be fixed a-priori from known noise variance

- the Sparse Signal Representation method is ideally suited for mode number analysis in fusion plasmas:
  - specifically designed for un-evenly distribution of sensors
  - allowable mode numbers are discretized: |n| = 0, ±1, ±2, ±3…
  - large (n,m)-range, number of modes not assumed a priori
  - amplitude and phase equally important for fitting algorithm
  - no need for a-posteriori tresholding to discriminate between solutions as λ-penalty determined a-priori from knowledge of noise variance
  - **implemented and fully validated in JET real-time and post-pulse mode tracking algorithm for stable Alfvén Eigenmodes**
  - **accuracy ➔ need correct interpretation of the spectral window**

Cost-Normalized Measurement Performance for the ITER HF Magnetic Diagnostic System

- overall procurement (R&D, design, prototyping, series manufacturing, post-production testing), installation and data acquisition costs as a further guideline to “optimize” the number and position of the in-vessel HF magnetic sensors for ITER
- due to the existing uncertainties on the design of the ITER vacuum vessel and its cabling interfaces here we use a very simplified model to evaluate this cost function, which is based on these assumptions (with a range for their values), from our experience on JET and TCV:
  - each individual sensors costs 7→10 cost-units end-to-end, i.e. from design to manufacturing to installation to the final data acquisition
  - each high-resolution sensor in any of the equatorial ports bears an additional installation cost of 1→2 cost-units due to the different needs for mechanical fixing, requiring further R&D work
  - each poloidal sensor located in the regions $60<\theta(\text{deg})<120$ and $270<\theta(\text{deg})<315$ bears an additional installation cost of 1→2 cost-units, due to more difficult cabling access
  - each high-field side poloidal sensor located in the region $120<\theta(\text{deg})<220$ bears an additional installation cost of 2→3 cost-units, again due (even) more difficult cabling access
  - each high-field side poloidal sensor located in the divertor region $220<\theta(\text{deg})<270$ bears an additional installation cost of 4→7 cost-units, again due to (even) more difficult in-vessel cabling access and to need for improved RF screening of image and eddy currents
  - finally, if we have more than 8 toroidal sensors (including high-resolution ones) in any one of the 9 machine sectors, the cost increases by 1→2 cost-units for each additional group of 8 sensors due to need of installing one further cabling loom in that sector

How ITER Intends to Measure the Spectrum of High-Frequency MHD Instabilities so as to satisfy the Measurement Requirements?

- for toroidal mode number detection: 2 arrays of 2x18 sub-assemblies with equi-spaced sensors on the low-field side
- for poloidal mode number detection: 6 arrays of 16 un-evenly spaced sensors (with divertor region blacked-out)
- can add high-resolution arrays inside any of the 18 equatorial ports (2 ports on each machine sector)
- **purpose of our work: these 2 and 6 further alternative geometries designed and tested on simulated ITER data**
- **note: measurement performance normalized with respect to estimated R&D and installation costs**

Baseline System Design for the ITER HF Magnetic Diagnostic

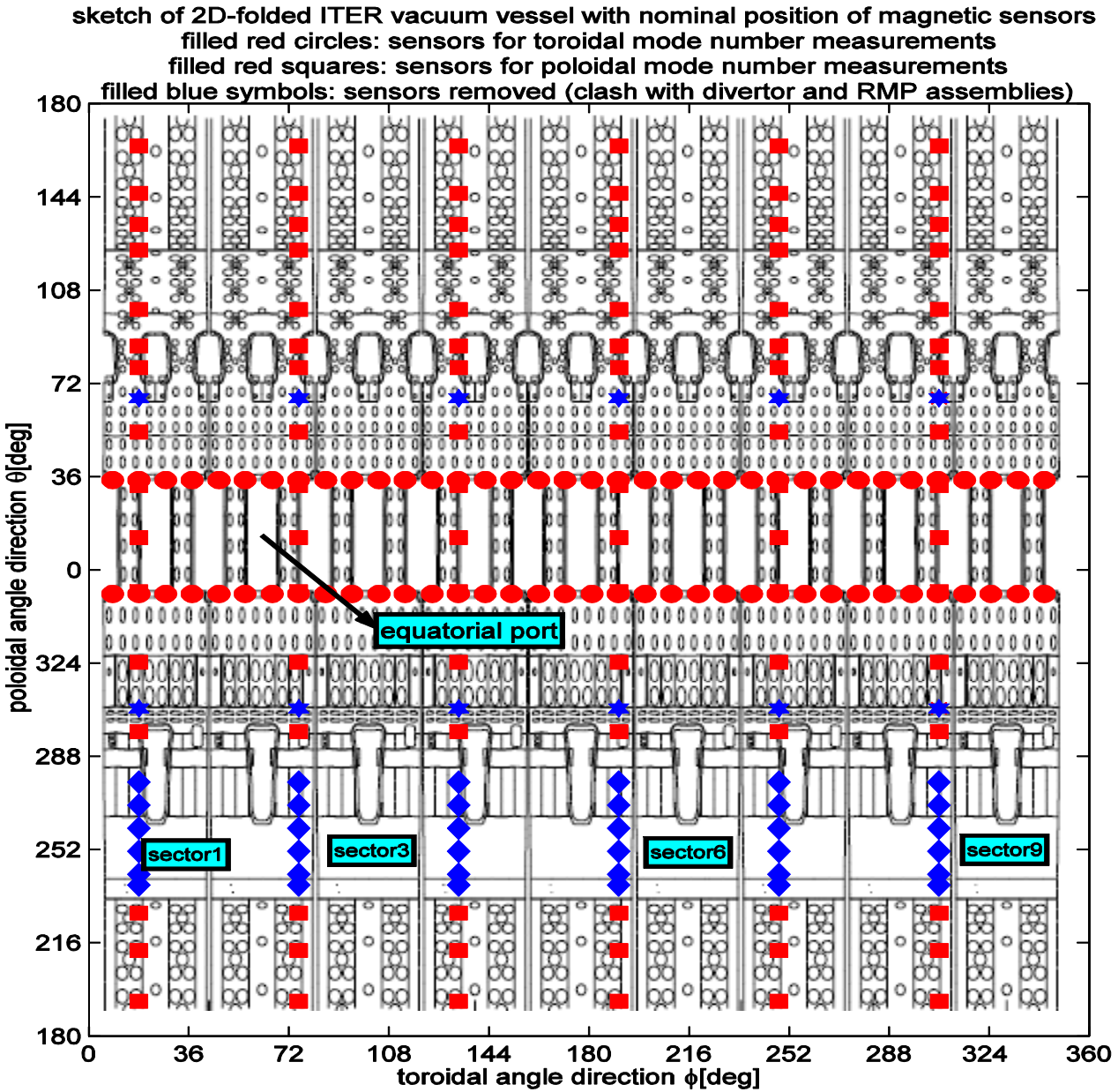

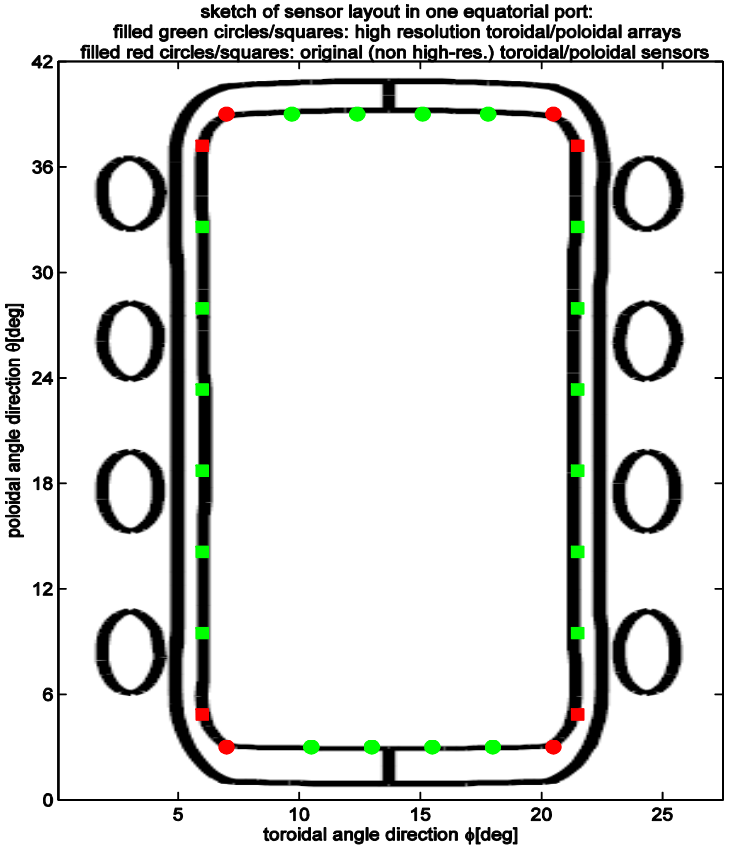

Test Configurations for the ITER HF Magnetic Diagnostic System

V1: baseline array with NN equi-spaced baseline sensors, to be used both for n- and m-number detection; additional equi-spaced array(s) with N_{HR} sensors each can be added inside the selected NP-th equatorial port(s).
V2: baseline array with NN randomly positioned baseline sensors, to be used both for n- and m-number detection; additional randomly spaced array(s) with N_{HR} sensors each can be added inside the selected NP-th equatorial port(s).
V3: baseline geometry for the ITER n-number array using NN=2x18=36 sensors in total; the array is made up of two equi-spaced sub-assemblies positioned on the corners (at the same Z) of each equatorial port; additional equi- or randomly spaced array(s) with N_{HR} sensors each can be added inside the selected NP-th equatorial port(s).
V4: baseline geometry for the ITER n-number array using 6 sensors in total, i.e. those located at the same Z from the m-number arrays on the 6 chosen machine sectors.
V5: baseline geometry for the ITER m-number array using the whole set of 24 non equi-spaced sensors, which are located on 6 different machine sectors (sectors [1, 2, 4, 5, 7, 8] when using the convention defined in fig1); one additional equi- or randomly spaced array with N_{HR} sensors can be added inside the equatorial port on the selected machine sector(s).
V6: as V5 but now considering the clashes with the RMP assemblies, hence using 22 non equi-spaced sensors in total on 6 machine sectors; one additional equi- or randomly spaced array with N_{HR} sensors can be added inside the equatorial port on the selected machine sector(s).
V7: as V5 but with the divertor region blacked-out, hence using 18 non equi-spaced sensors in total plus one additional equi- or randomly spaced high-resolution array with N_{HR} sensors.
V8: as V6 but with the divertor region blacked-out, hence using 16 non equi-spaced sensors in total plus one additional equi- or randomly spaced high-resolution array with N_{HR} sensors.

Sensor Configurations for Toroidal Mode Number Detection

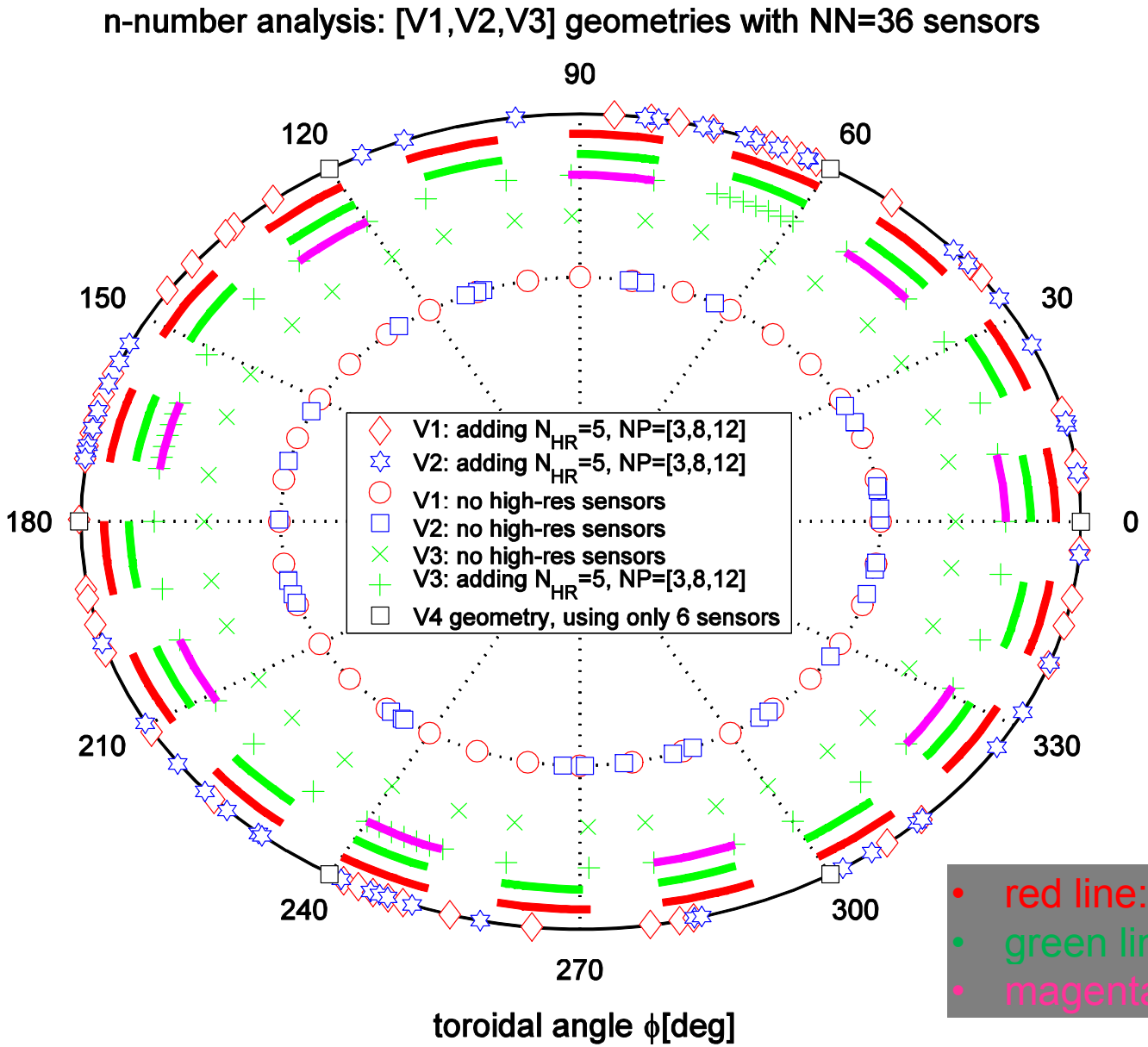

- illustrative layout for the baseline geometries [V1, V2, V3] for toroidal mode number analysis using NN=36 sensors with/out adding NHR=5 high resolution sensors in the three equatorial ports NP=[3,8,12];
- also shown the layout of the V4 baseline geometry, which has only 6 sensors, as obtained using the sensors located at the same height Z on the low-field side wall in the six poloidal arrays described by the V8 geometry

- red line: lower midplane port
- green line: equatorial port
- magenta line: upper midplane port

Sensor Configurations for Poloidal Mode Number Detection

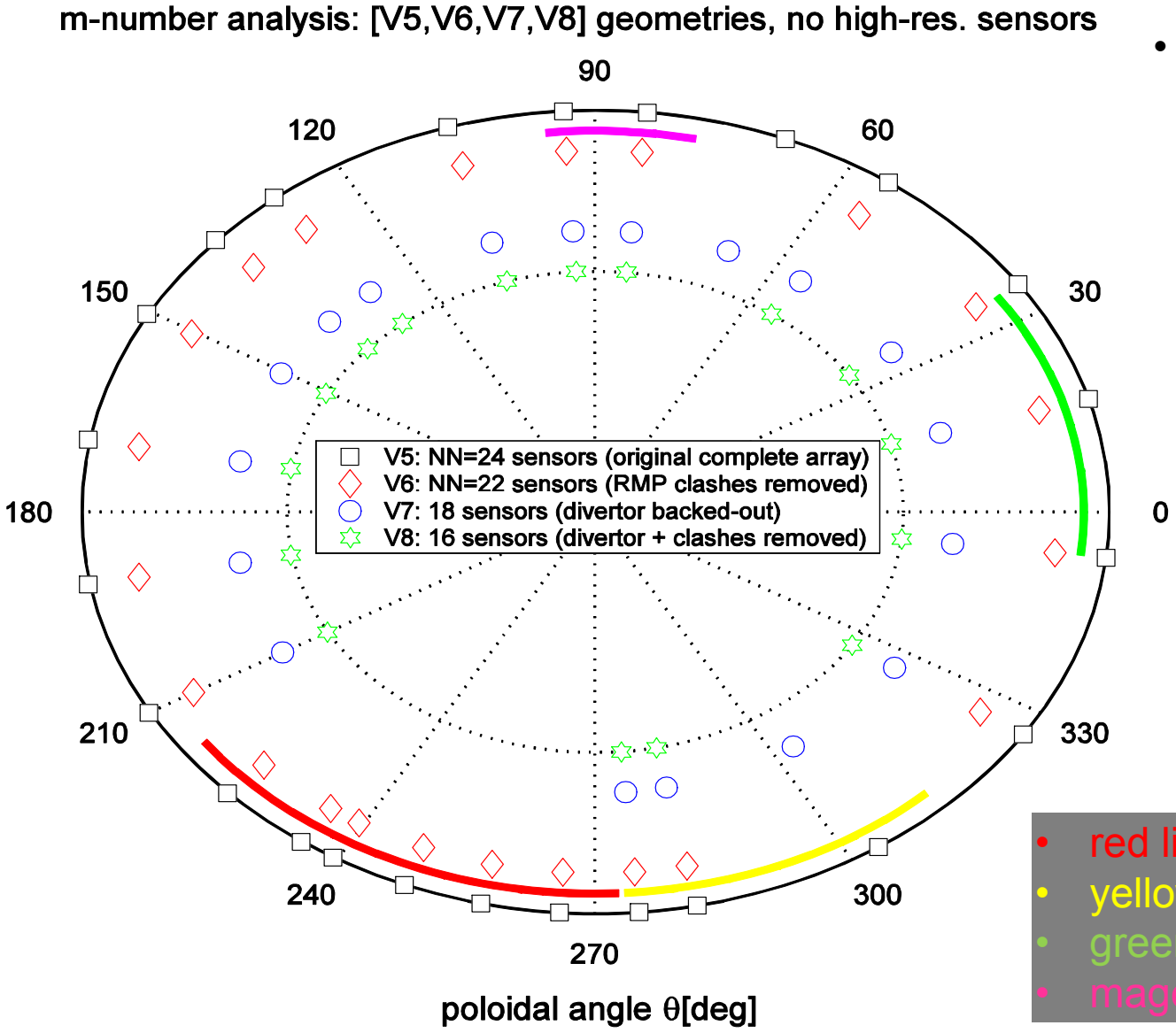

- illustrative layout for the [V5, V6, V7, V8] baseline geometries for poloidal mode number analysis, without the addition of high resolution sensors in the equatorial port intersected by these baseline measurement arrays

- red line: divertor shadow
- yellow line: lower mid-plane port
- green line: equatorial port
- magenta line: upper mid-plane port

Sensor Configurations for Poloidal Mode Number Detection

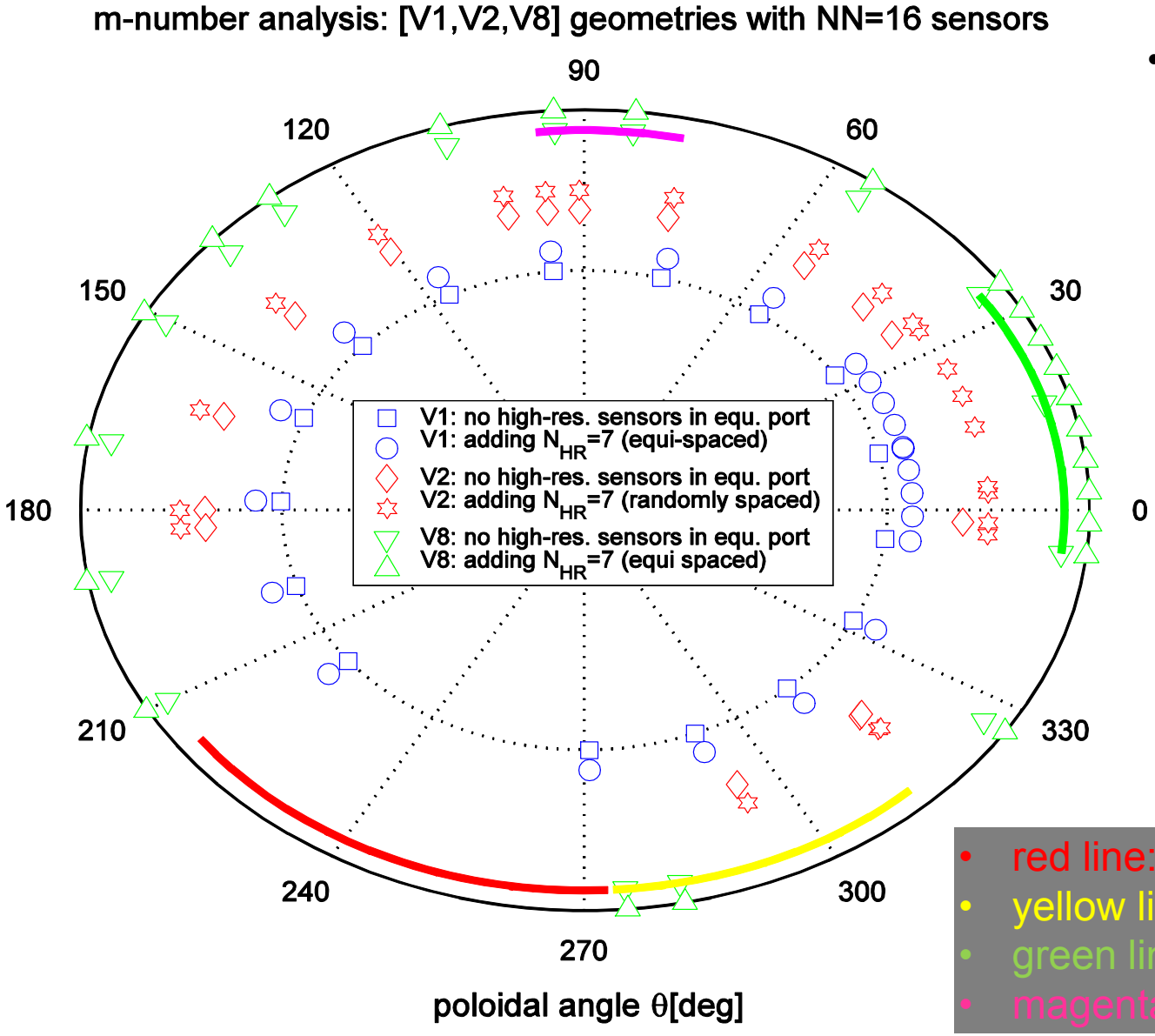

- illustrative layout for the [V1, V2, V8] baseline geometries for poloidal mode number analysis, shown here using NN=16 with/out adding NHR=7 high resolution sensors in the relevant equatorial port, respectively, and always blacking-out the divertor region

- red line: divertor shadow (blacked-out)
- yellow line: lower mid-plane port
- green line: equatorial port
- magenta line: upper mid-plane port

Sensor Configurations for Poloidal Mode Number Detection

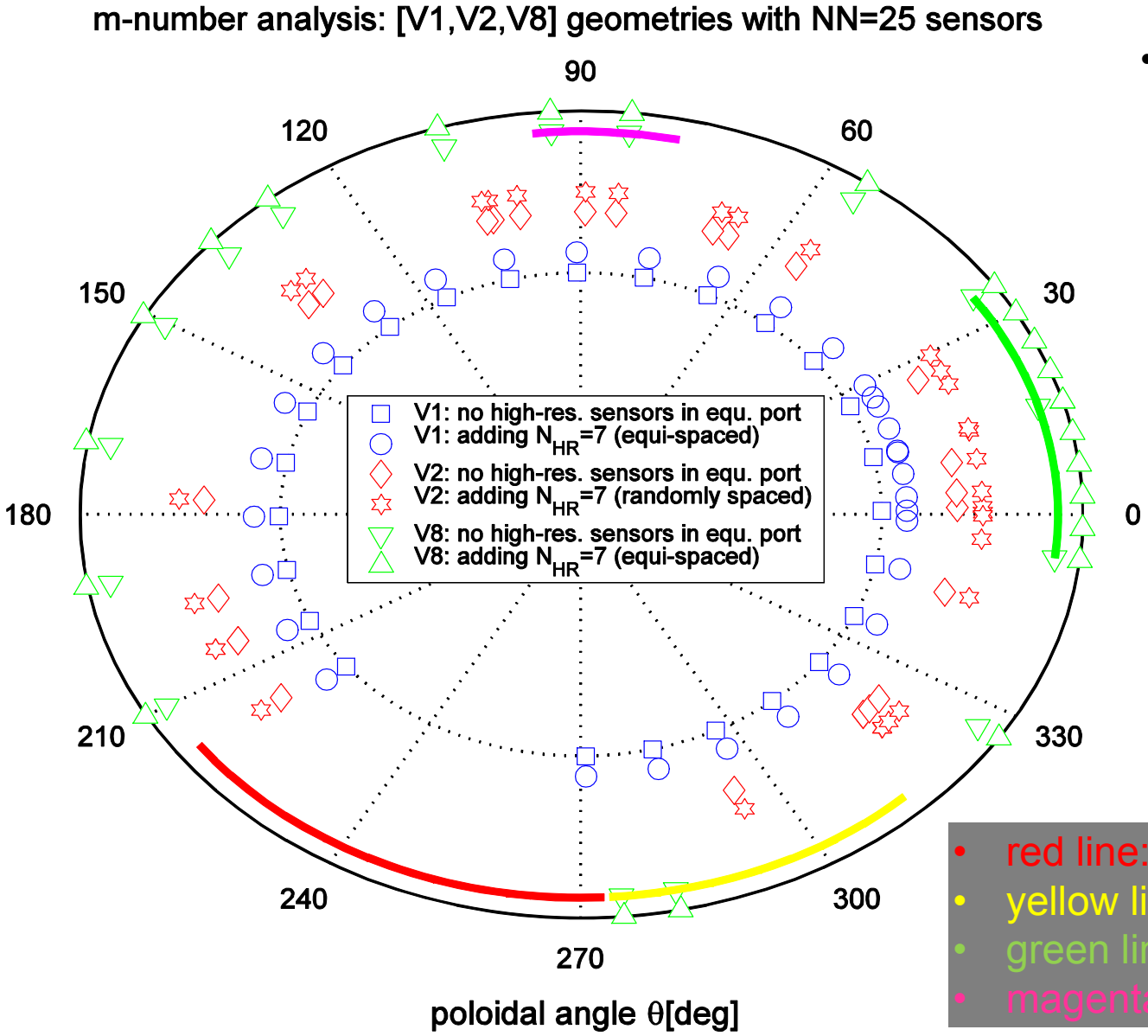

- illustrative layout for the [V1, V2, V8] baseline geometries for poloidal mode number analysis, shown here using NN=25 with/out adding NHR=7 high resolution sensors in the relevant equatorial port, respectively, and always blacking-out the divertor region

- red line: divertor shadow (blacked-out)
- yellow line: lower mid-plane port
- green line: equatorial port
- magenta line: upper mid-plane port

Construct the Input Signal at the Position of the Sensors

- start with an arbitrary sum of components with amplitude $A_k \in [0,1]$, integer frequency ($\equiv$ mode number) $f_k \in [-f_{MAX}, +f_{MAX}]$, relative phase $\delta_k \in [0,2\pi]$
- $\{A_k, f_k, \delta_k\}$ can be fixed or randomized (each one independently)
- add random noise on the input spectrum with standard deviation σ_{SIG} due to physics: background un-coherent turbulence, …
- add random noise on the measurement with standard deviation σ_{MEAS} due to engineering: error on the position and alignment of the sensor, calibration errors, {cross-talk, drifts, offset, noise, …} in the cabling & electronics, …
- map the input spectrum at the position $t_p \in [0,2\pi]$ of each sensor: t_p is fixed for each simulation but changes if the simulation is re-run for a different number of sensors for the same type of geometry (un-/even spacing) unless constrained otherwise

$$S_{IN}(t_p) = \left[\sum_{k=-f_{MAX}}^{k=+f_{MAX}} A_k \exp\left(i f_k t_p + i\delta_k \right) + \sigma_{SIG} \times \left(r_{1k} + i r_{2k} \right) \right] + \sigma_{MEAS}(t_p) \times \left(r_{3p} + i r_{4p} \right)$$

- $\{r_{1k}, r_{2k}, r_{3p}, r_{4p}\}$ are random numbers chosen from a uniform distribution in [0.0→1.0]
- the random seed used for $\{r_{1k}, r_{2k}\}$ can be different from the one for $\{r_{3p}, r_{4p}\}$
- the values for $\sigma_{SIG} \in [0,1]$ and $\sigma_{MEAS} \in [0,1]$ can also be different
- the values for $\sigma_{MEAS}(t_p)$ can also be different for different sensors

Constraints for the Simulations

- **to comply with the installation requirements:**
  - **MUST** keep the same geometry (un-/even spacing) when changing the number of sensors
  - **CAN** only mix geometries when adding high-resolution array(s) in the equatorial port(s)
  - **MUST** respect pre-selected unusable zones: divertor, ports, etc…
- **to comply with the measurement requirements:**
  - **no weight** on the individual measurement points: all data have the same use independently of where they are obtained (blind analysis)
  - **BUT weight** on the number (and position) of sensors used to achieve measurement performance ➔ minimization of the installation costs
  - **AND biased estimation of the results of the simulations**

  ➔ the solution $\{A_{OUT}, f_{OUT}\}$ is classified as **CORRECT** only if the differences $\{|A_{OUT}-A_k|, |f_{OUT}-f_k|\}$ with the input are **BOTH** within the set tolerances, otherwise the solution is classified as **WRONG**

  ➔ **this is VERY DIFFERENT from the usual un-biased estimation of the measurements, and leads to rather un-expected results…**

Simulations Run for the ITER HF Magnetic Diagnostic System

- many different implementations for each of the possible geometries by changing:
  - the number and position of non-high resolution sensors
  - with/out adding high-resolution array(s) in the equatorial port(s)
  - with/out blacking-out the divertor region for poloidal mode number analysis
  - with/out blacking-out poloidal angles in the range $75<|\theta|(\text{deg})<105$ (because of the θ_*-correction to the sensors' position)
- many different simulations run using each of the possible geometries by changing:
  - the number of the modes in the input spectrum
  - the relative amplitude, phasing and frequency
  - the maximum frequency to be detected
  - the amount of background noise (additive: more modes/sensors ➔ more noise)
- in total we used for this work:
  - four different ITER reference magnetic equilibria
  - ~330 different implementations for the eight test geometries
  - ~49'000 different simulations for the four optimization tests
  - ~115 days of CPU time using Matlab R-12 on a laptop with a 1.5GHz Intel processor and 1GB of RAM

Noise Rejection Tests: Purpose

- **purpose of these tests:** understand the sensitivity of the possible geometries for the ITER HF magnetic diagnostic system with respect to false detection of modes as function of the level of background noise
  - ➔ *i.e.: noise being mistaken for a "true" plasma mode because of the specific sensors' arrangement*
- this problem is of high significance in the framework of non-uniform sampling theory as it is definitively not foreseeable for ITER to have a sufficient number of equi-spaced in-vessel HF magnetic sensors for the spatial Nyquist frequency to exceed the maximum (n,m)-mode that needs to be accurately detected
  - ➔ *paramount to understand if a specific sensor arrangement is more prone to false mode detection from noise-only data than the others*
- **outcome of these simulations:** determine an a-priori confidence level in mode detection for each possible geometry for the ITER HF magnetic diagnostic system
  - ➔ *corresponds to identify an a-priori "cost function" to reduce the occurrence of noise-driven mode detection by 5% for each possible geometry*

Noise Rejection Tests: Results

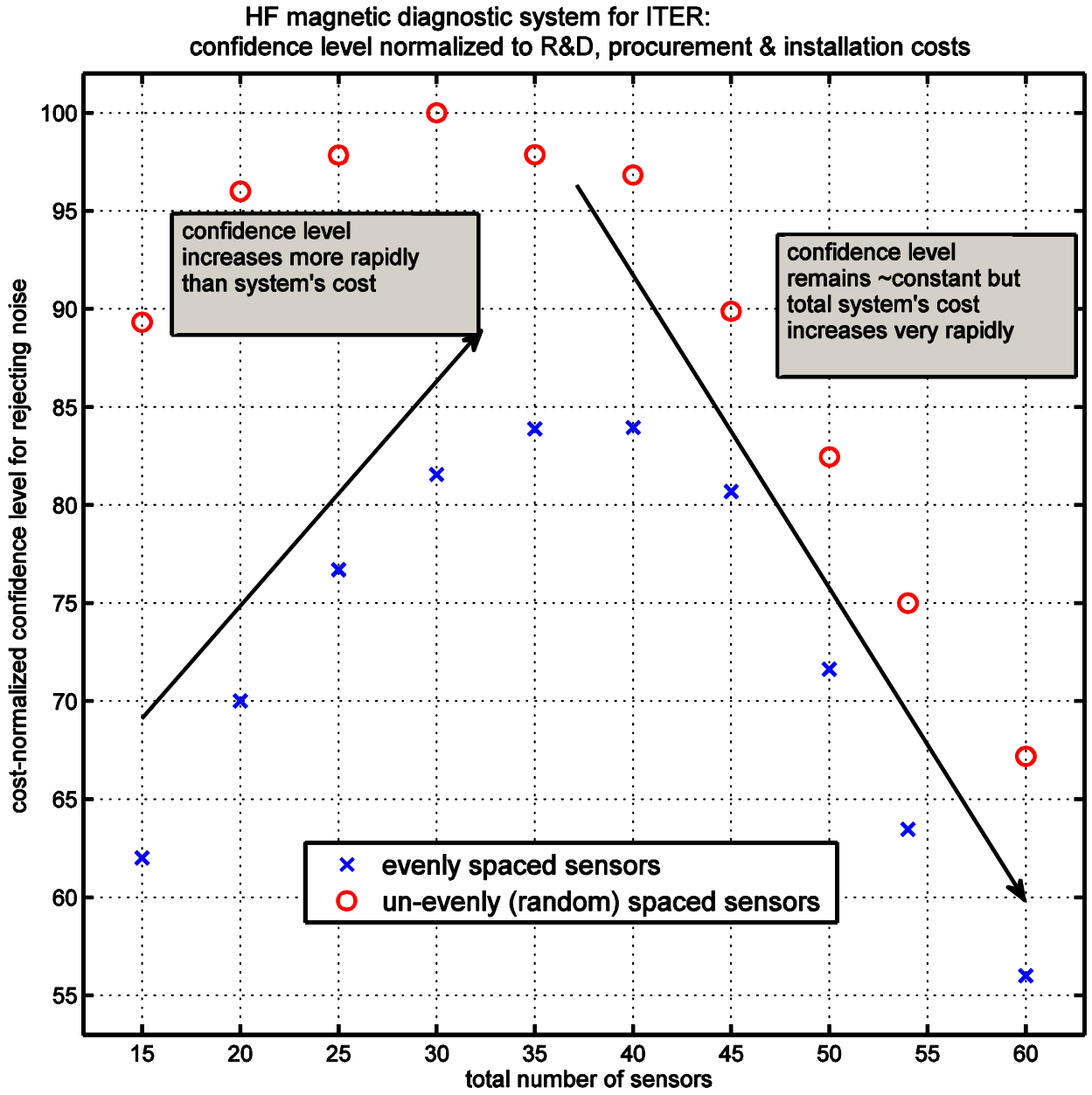

measurement performance normalized wrt estimated installation costs

1. maximum in confidence level ≡ minimum in cost function for noise rejection
2. minimum in cost function obtained with ~30 un-evenly spaced sensors (V2)
3. minimum in cost function only obtained with ~40 evenly sensors (V1)
4. confidence level decreases (≡ cost function increases) for an even higher number of sensors as measurements errors start to dominate over the reduced sensor spacing

Noise Rejection Tests: Summary Conclusions

1. equi-spaced sensor geometries (or made up with sub-assemblies with spatial periodicities) (➔ as the ITER nominal geometry for toroidal mode number detection) are more prone to noise-driven false detection of high-n(m) modes
   ➔ *situation only marginally improved by adding high-resolution array(s) inside the equatorial port(s)*
2. truly random sensor arrangements are very robust against noise-driven false detection of high-n(m) modes provided the spatial coverage is sufficiently complete
   ➔ *adding high-resolution array(s) inside the equatorial port(s) does not produce any further improvement*
3. if the spatial coverage leaves significantly large regions blacked-out (➔ as the ITER nominal geometry for poloidal mode number detection), such as the divertor region when considering poloidal mode number analysis, adding a few (5-7) sensors in high-resolution array(s) inside the equatorial port(s) improves the resilience against mistakenly detecting white noise for high-n(m) modes
4. the best use of high resolution array(s) inside the equatorial port(s) is to have a relatively small number of sensors (5-7) in non equi-distant ports which are as far apart as possible

False Alarms Avoidance Tests: Purpose

- **purpose of these tests**: answer the following questions:
  1. what is the probability that we can correctly detect the input mode spectrum using the given sensor arrangement?
  2. what is the precision on the amplitude of the correctly detected modes?
  3. what is the probability of false alarms (i.e.: detection of a mode which is not in the input spectrum)?
  4. how high are the amplitudes and what are the mode numbers of these false alarms?
- **outcome of these simulations**: identify the arrangements of sensors that give the higher number of correctly detected modes and the lower number of false alarms with the lowest possible amplitude for mode numbers not of interest for real-time protection and control applications

➔ **these configurations are the best "nominal" choice for in-vessel installation**

False Alarms Avoidance Tests: n-Results

(measurement performance normalized wrt estimated installation costs)

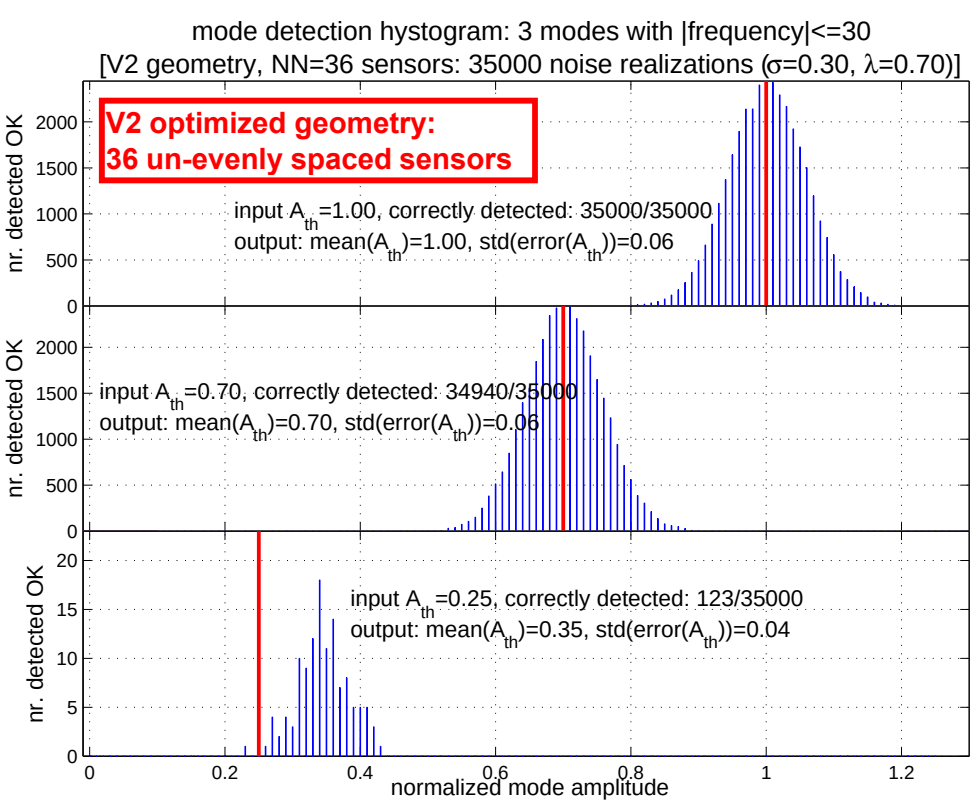

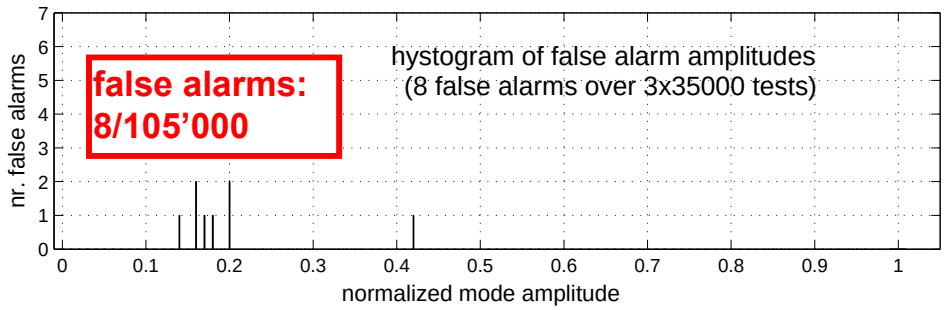

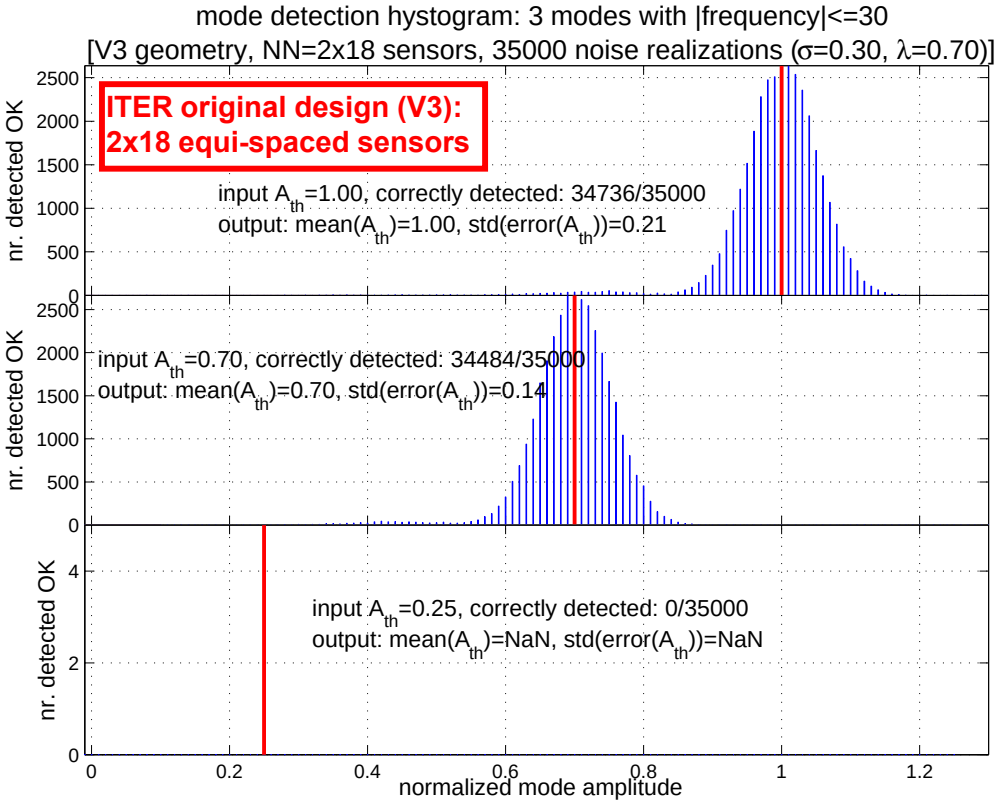

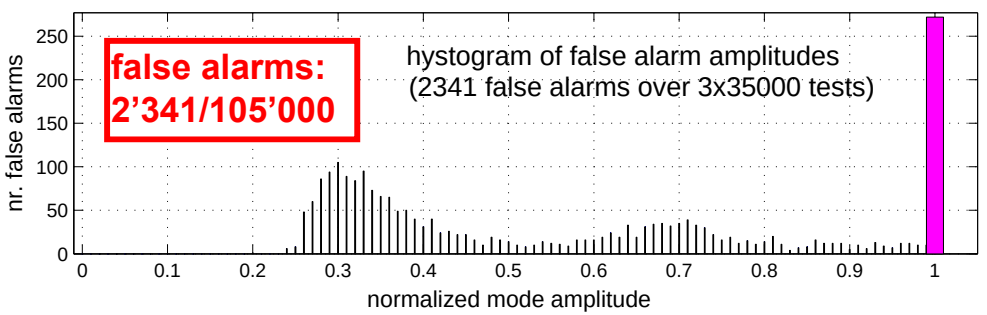

- **false alarms: modes have been detected which are not in the input spectrum**
- **very low number of false alarms for the optimized V2 geometry: either the modes are correctly detected, or are not detected at all ➔ fail-safe diagnostic system**

False Alarms Avoidance Tests: n-Results

(measurement performance normalized wrt estimated installation costs)

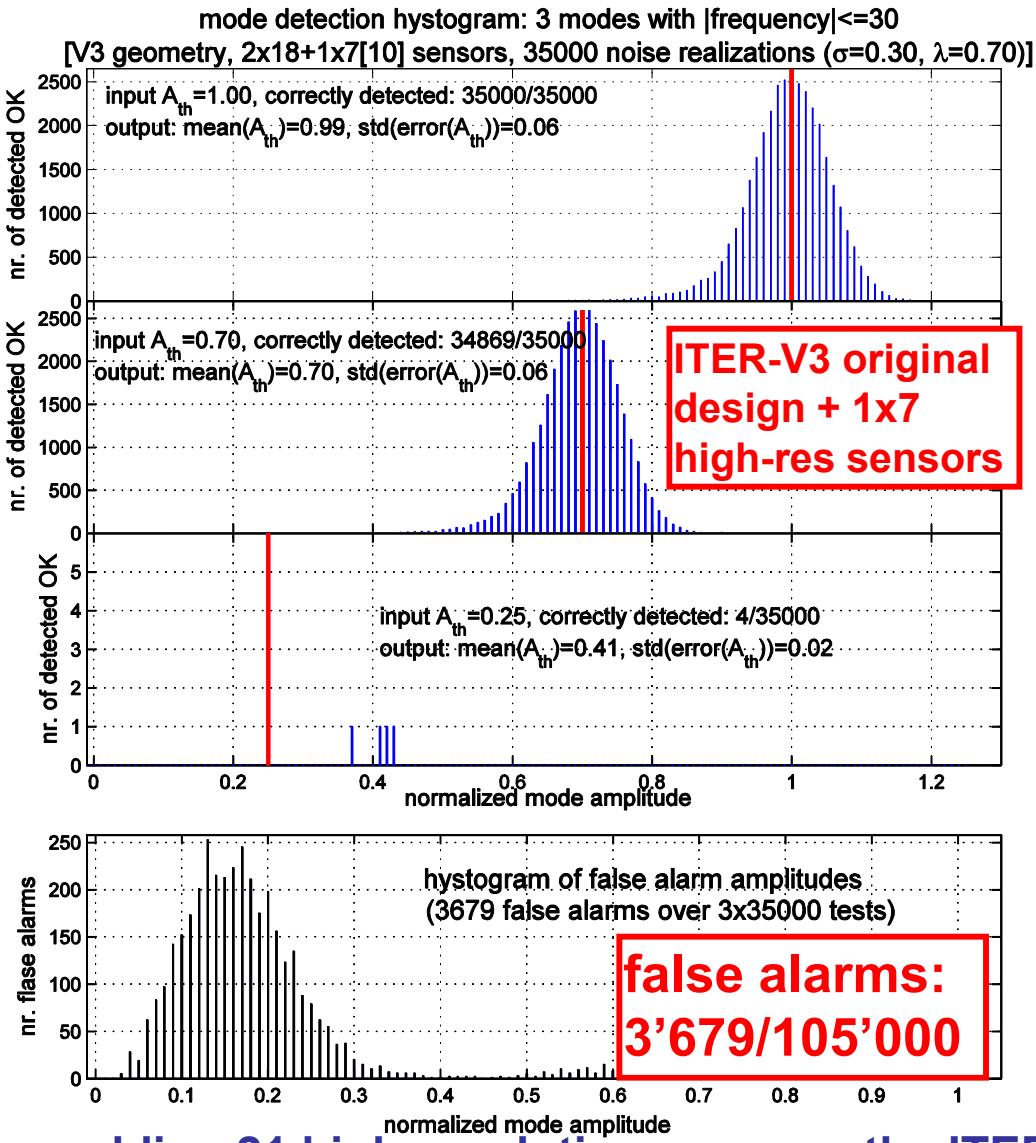

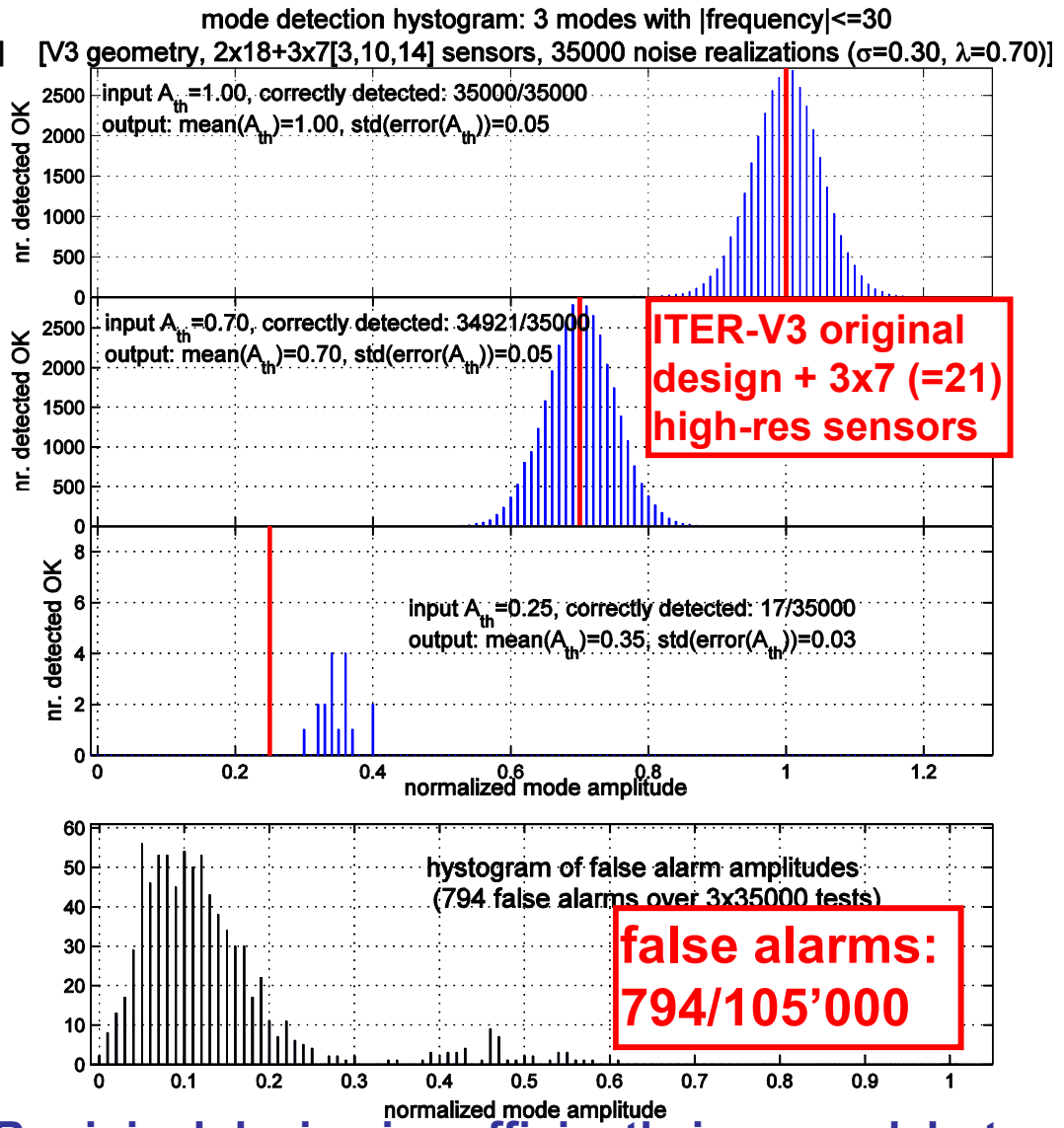

- adding 21 high-resolution sensors, the ITER original design is sufficiently improved, but not performing as optimized V2 geometry because of its original 2x18 Nyquist periodicity
- with optimized V2 geometry: only 8/105'000 false alarms

False Alarms Avoidance Tests: n-Results

- the number of false alarms is not only lower for the V2 geometry, but it is also essentially independent on the number of high-resolution sensors
- the number of false alarms initially decreases for the V1 and V3 geometries as up to ~7 high-resolution sensors are added
- then it starts increasing for an even higher number (>7) of high-resolution sensors
- results averaged over many simulations: 2→5 input modes (35'000 realization tests each), noise variance σ=0.0→0.3, fixed λ_{FIT}=0.7 and f_{MAX}=30

measurement performance normalized wrt estimated installation costs

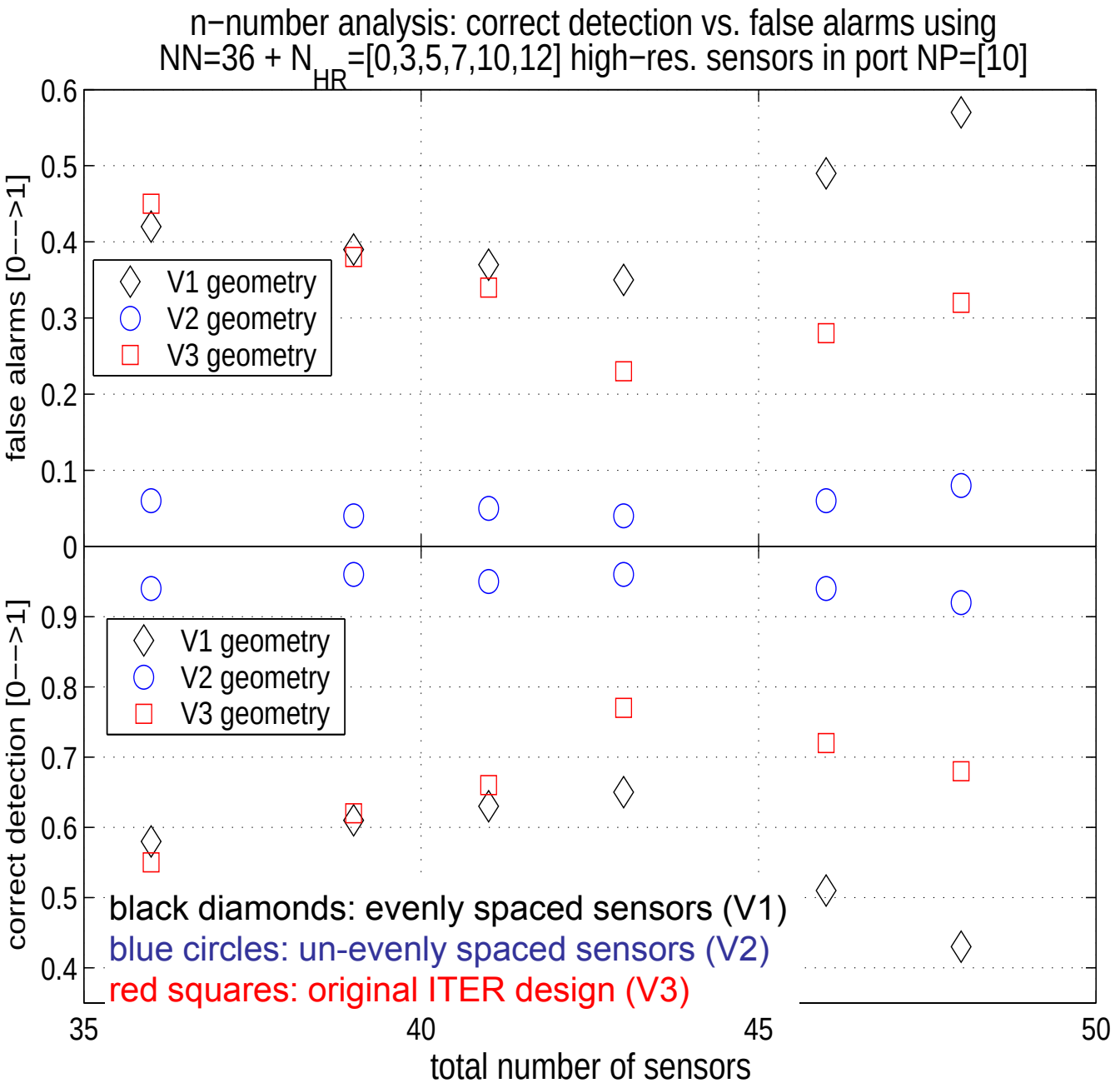

False Alarms Avoidance Tests: n-Results

(measurement performance normalized wrt estimated installation costs)

NN	NHR	NP	FalseAlarms V2	DetectedOK V2	FalseAlarms V3 (ITER)	DetectedOK V3 (ITER)
36	**0**	**[0]**	**0.06**	**0.94**	**0.45**	**0.55**
36	3	[3]	0.05	0.95	0.39	0.61
36	3	[10]	0.04	0.96	0.38	0.62
36	3	[14]	0.04	0.96	0.39	0.61
36	5	[3]	0.04	0.96	0.33	0.67
36	5	[10]	0.05	0.95	0.34	0.66
36	5	[14]	0.03	0.97	0.32	0.68
36	7	[3]	0.04	0.96	0.25	0.75
36	**7**	**[10]**	**0.04**	**0.96**	**0.23**	**0.77**
36	7	[14]	0.05	0.95	0.24	0.76
36	10	[3]	0.05	0.95	0.28	0.72
36	10	[10]	0.06	0.94	0.28	0.72
36	10	[14]	0.05	0.95	0.27	0.73
36	12	[3]	0.07	0.93	0.32	0.68
36	12	[10]	0.08	0.92	0.32	0.68
36	12	[14]	0.09	0.91	0.31	0.69
36	**5**	**[3,10,14]**	**0.07**	**0.93**	**0.15**	**0.85**
36	5	[9,10,11]	0.10	0.90	0.20	0.80
36	5	[6,10,12]	0.08	0.92	0.16	0.84

- statistical analysis on calculation of n's:
- V3 (original system design) vs.
- V2 (randomly spaced sensors)

1. un-acceptably large number of false alarms for V3 (original)
2. V3 becomes *almost OK* by adding 3x7 high-res. sensors
3. **but still false alarms for V3 with 57 sensors are >twice those of V2 with only 36 sensors**
4. **V2 not much improved by adding high-res. sensors**

False Alarms Avoidance Tests: m-Results

(measurement performance normalized wrt estimated installation costs)

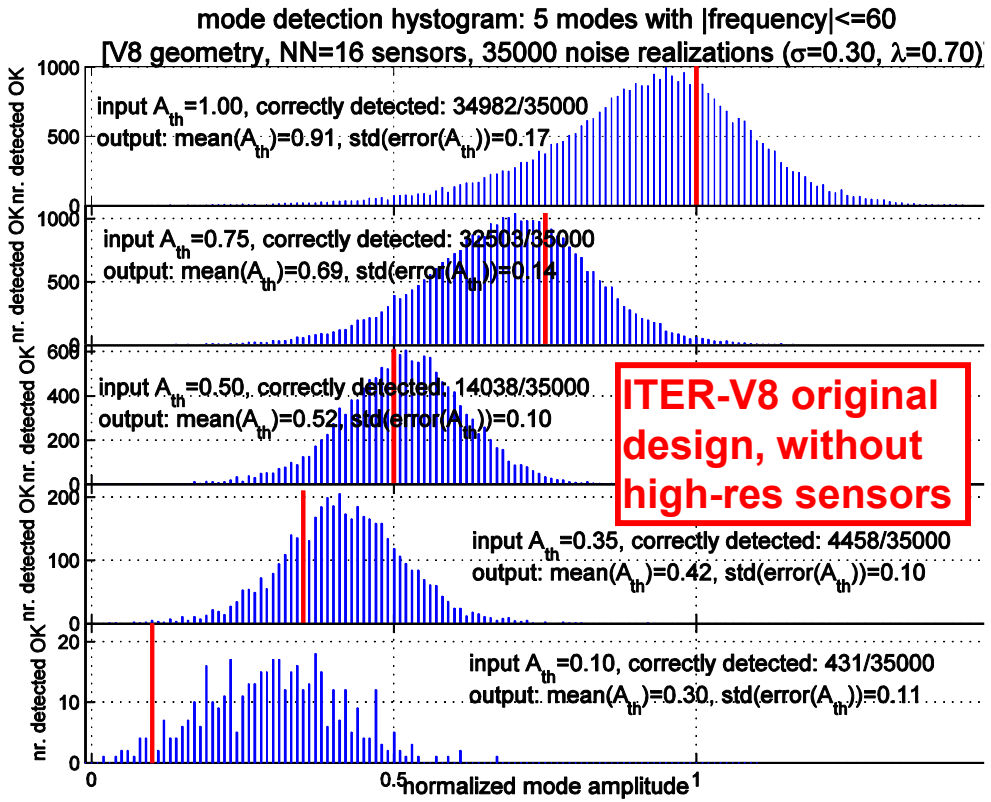

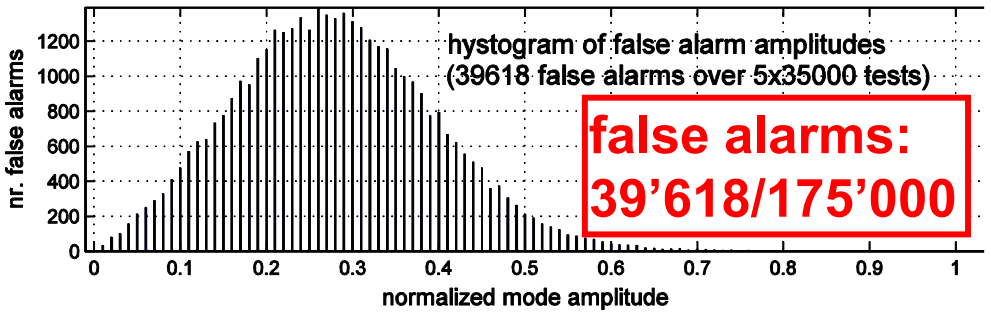

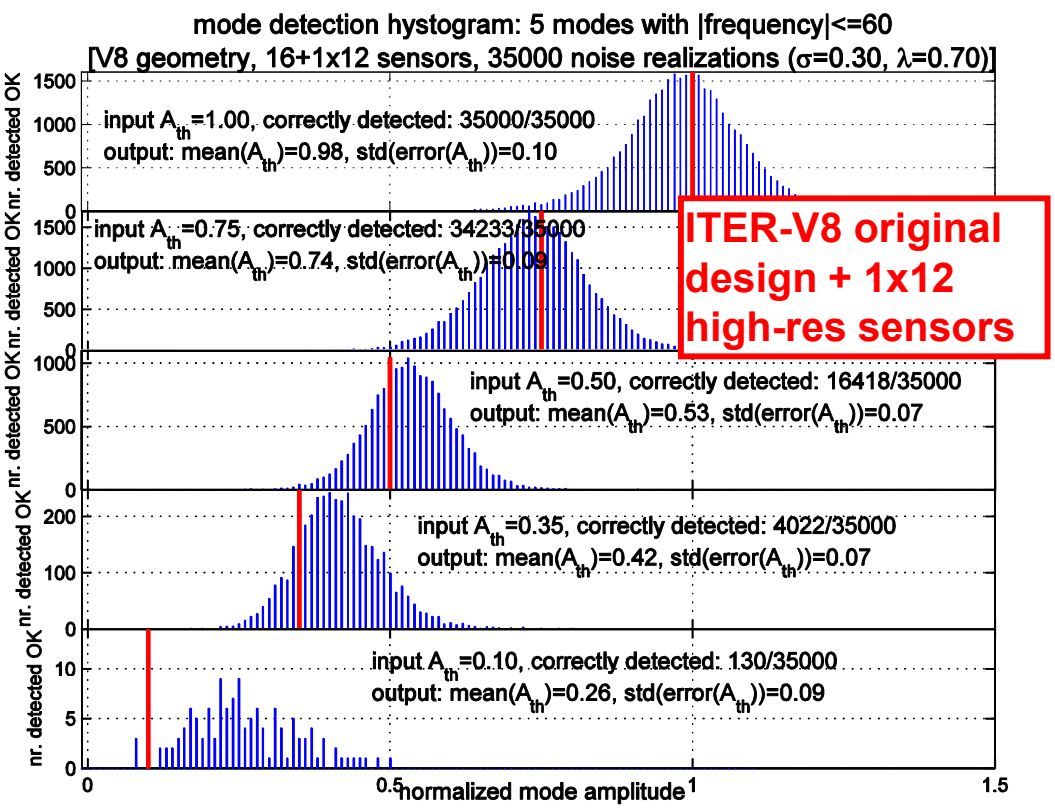

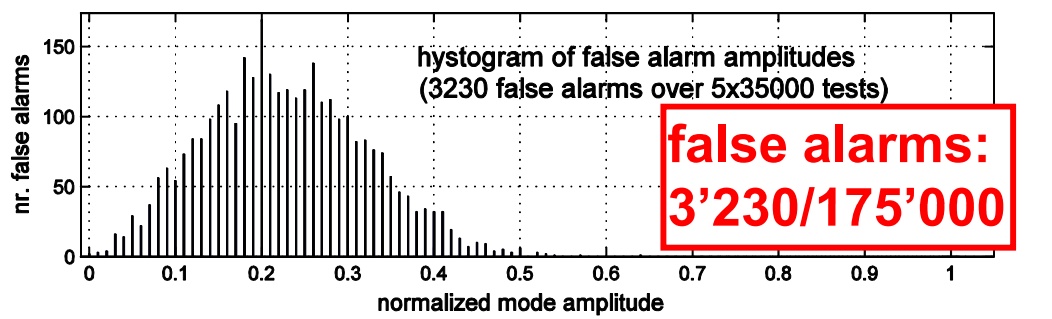

- **ITER original V8 geometry suffers from lack of sensors: >20% false alarms!!**
- **adding 12 high-resolution sensors in the equatorial port improves false alarms avoidance**

False Alarms Avoidance Tests: m-Results

- [V1, V2, V8] geometries have the same behavior when adding high-resolution sensors: initial improvement and then degradation of the measurement performance
- number of false alarms is lower for the V2 than for the V8 geometry; difference not as striking as the one obtained analyzing the V3 geometry
- original V8 geometry does not have major periodicities in the sensor arrangement; V2 and V8 geometries blacked-out in the divertor region
- results averaged over many simulations: 2→5 input modes (35'000 realization tests each), noise variance σ=0.0→0.3, fixed λ_{FIT}=0.7 and f_{MAX}=60

measurement performance normalized wrt estimated installation costs

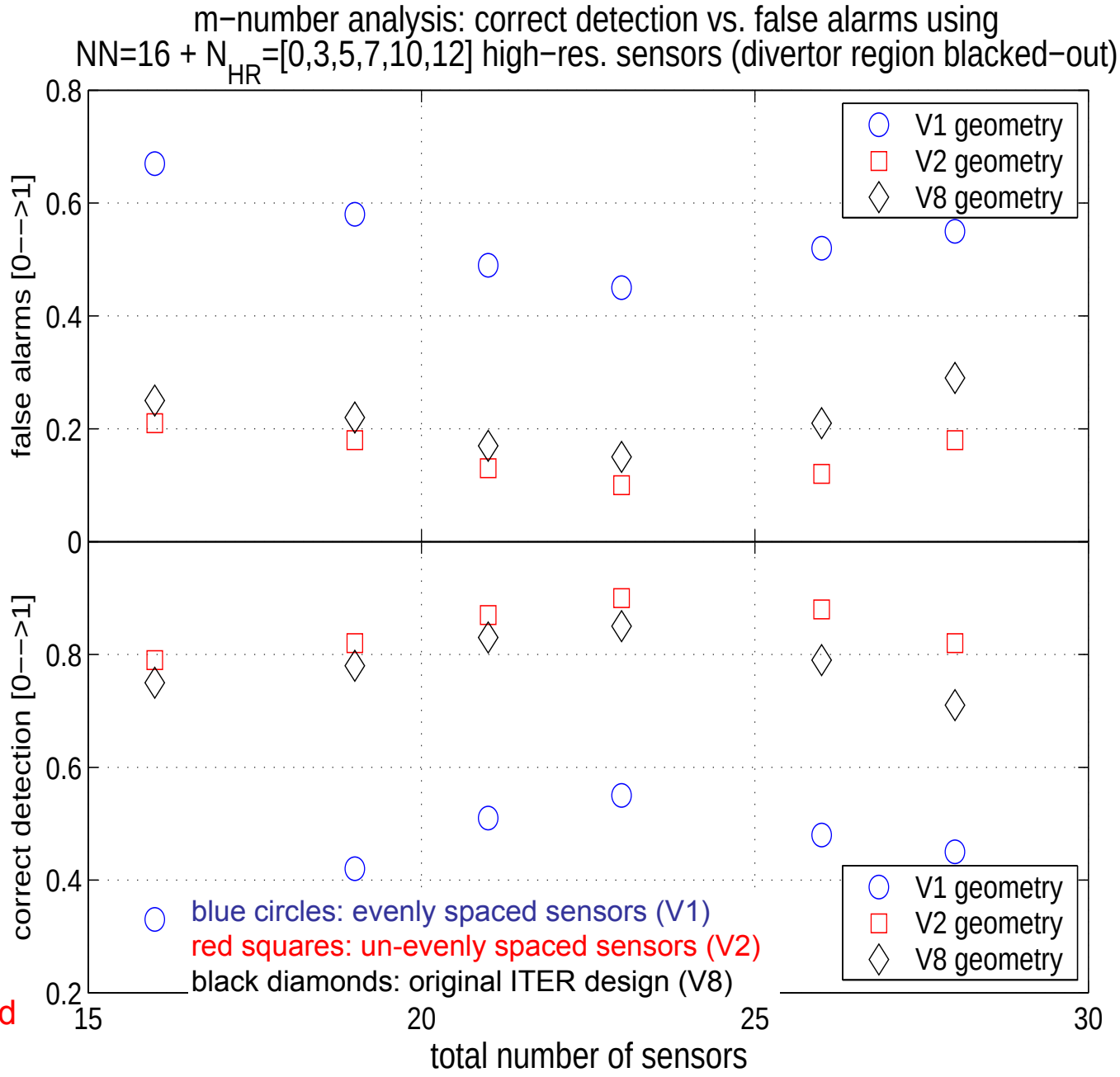

False Alarms Avoidance Tests: m-Results

(measurement performance normalized wrt estimated installation costs)

- statistical analysis on calculation of poloidal mode numbers:
  - V1 (equi-spaced sensors) vs. V2 (randomly spaced sensors) vs. V8 (ITER current nominal system design, some hidden periodicities)
  - adding one high-resolution array in the equatorial port

NN	NHR	NP	V1: False Alarms	V1: Correct Detection	V2: False Alarms	V 2: Correct Detection	V8 (ITER): False Alarms	V8 (ITER): Correct Detection
16	**0**	**[0]**	**0.67**	**0.33**	**0.21**	**0.79**	**0.25**	**0.75**
16	3	[10]	0.58	0.42	0.18	0.82	0.22	0.78
16	5	[10]	0.49	0.51	0.13	0.87	0.17	0.83
16	**7**	**[10]**	**0.45**	**0.55**	**0.10**	**0.90**	**0.15**	**0.85**
16	10	[10]	0.52	0.48	0.12	0.88	0.21	0.79
16	12	[10]	0.55	0.45	0.18	0.82	0.29	0.71

- **equi-spaced geometry V1 has un-acceptably high number of false alarms**
- **truly random geometry V2 performs better that original V8 (ITER)**
- **addition of high resolution sensors beneficial provided not too closely spaced**

False Alarms Avoidance Tests: σ-Results

(measurement performance normalized wrt estimated installation costs)

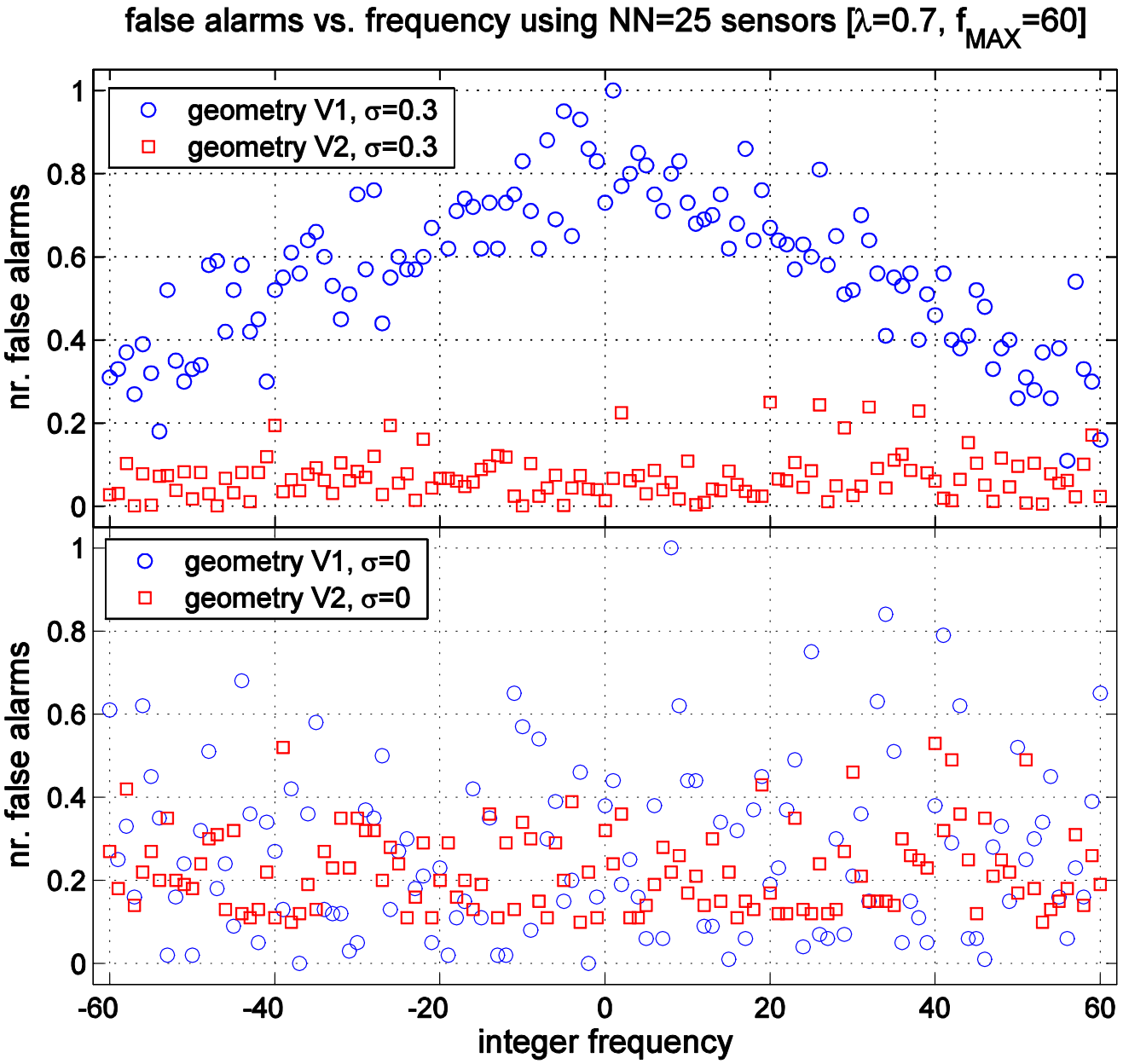

distribution of the false alarms frequency for NN=25 baseline and no high-resolution sensors for two values of the noise standard deviation σ=0 and σ=0.3 for the V1 and V2 geometries:

1. for σ=0 the V2 and V1 geometries performs equivalently;
2. for σ=0.3 the V2 geometry is much less sensitive to false alarms than the V1 geometry;
3. for σ=0.3 also different frequency distribution: still flat for V2, whereas the V1 geometry fails more in rejecting false alarms at low frequency

False Alarms Avoidance Tests: Summary Conclusions

1. any periodicity in the sensors' spatial arrangement makes the system more prone to false alarms
   - ➔ *it is completely unpractical to install a sufficient number of sensors for the spatial Nyquist criterion to become fully applicable*
2. already limited amount of background noise variance contribute to deteriorate the cost-normalized measurement performance for multiple mode detection ➔ larger effect on geometries with spatial periodicities
3. detection of poloidal mode numbers: blacking-out the divertor region significantly reduces the spatial coverage and intrinsically adds an equivalent 50deg zero-signal periodicity to the measurements
4. the addition of high resolution array(s) inside the equatorial port(s) is only beneficial in reducing the occurrence of false alarms provided the separation between these sensors is sufficiently high for the measurements to be only marginally affected by the background noise

Resilience to Loss of Sensors: Purpose

- **purpose of these tests**: verify that the loss of 10% faulty sensors does not overly degrade the measurement performance of any given configuration that gives good results in terms of correct detection and false alarms when all sensors are working

$$\text{scatter error} = \frac{\frac{1}{N_{SIMUL}} \sum_{jj=1}^{N_{SIMUL}} \frac{1}{(N_{GOOD})_{jj}} \sqrt{\sum_{kk=1}^{(N_{GOOD})_{jj}} (signal_{kk} - fit_{kk})^2}}{\frac{1}{N_{SENS}} \sqrt{\sum_{kk=1}^{N_{SENS}} (signal_{kk} - fit_{kk})^2}}$$

$$MAX\,(\text{scatter error}) \leq 1 + 10 \times \frac{N_{SENS} - N_{GOOD}}{N_{SENS}} \leq 2 \Rightarrow \text{geometry OK}$$

- **outcome of these tests**: identify those sensors' arrangements which are more resilient against the loss of sensors, i.e. whose measurement performance is less degraded when some sensors become faulty

Resilience to Loss of Sensors: n-Results

- not even adding 3x5 high resolution sensors the original V3 geometry is sufficiently robust to satisfy the measurement requirements
- the V2 geometry satisfies the measurement requirements already with 36 sensors
- the best use of high-resolution arrays is with 5-7 sensors in far apart equatorial ports
- results averaged over many simulations: σ=0.0→0.3, λ_{FIT}=0.7, f_{maxM}=20→30, f_{maxS}=30→50

measurement performance normalized wrt estimated installation costs

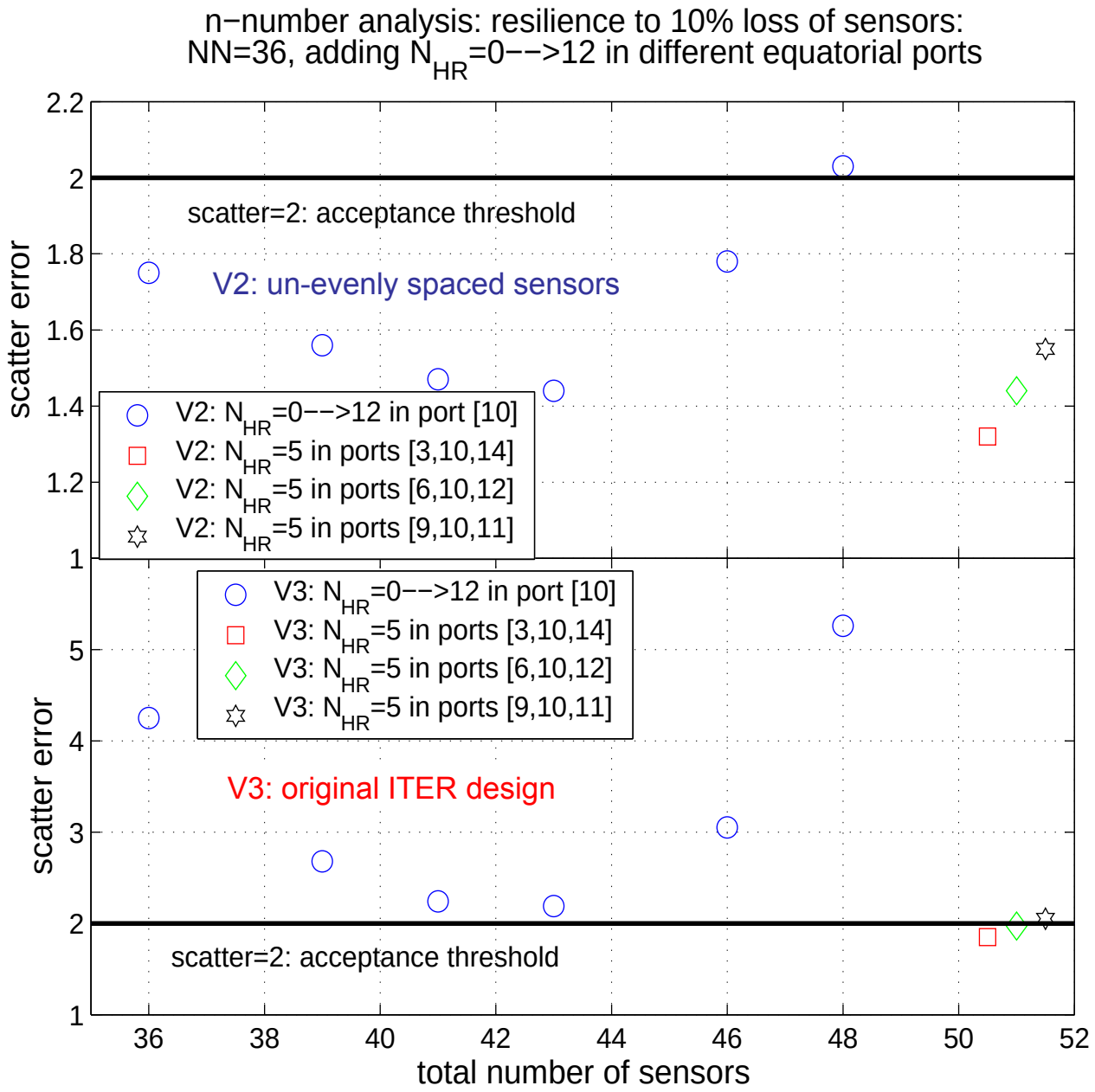

Resilience to Loss of Sensors: n-Results

geometry	NN	NHR	NP	scatter in normalized fit error for a 10% failure rate
V3	36	0	[0]	➔ scatter=4.25 >threshold=2 ➔ geometry not ok
V3	36	1x3	[10]	➔ scatter=2.68 >threshold=2 ➔ geometry not ok
V3	36	1x7	[10]	➔ scatter=2.19 >threshold=2 ➔ geometry not ok
V3	36	1x10	[10]	➔ scatter=3.05 >threshold=2 ➔ geometry not ok
V3	36	3x5	[3,10,14]	**➔ scatter=1.85 <threshold=2 ➔ geometry OK**
V3	36	3x5	[9,10,11]	➔ scatter=2.05 >threshold=2 ➔ geometry not ok
V2-n	18	0	[0]	➔ scatter=3.72 >threshold=2 ➔ geometry not ok
V2-n	18	1x3	[10]	➔ scatter=2.98 >threshold=2 ➔ geometry not ok
V2-n	18	1x7	[10]	**➔ scatter=1.92 <threshold=2 ➔ geometry OK**
V2-n	18	1x10	[10]	➔ scatter=2.07 >threshold=2 ➔ geometry not ok
V2-n	18	3x5	[3,10,14]	**➔ scatter=1.43 <threshold=2 ➔ geometry OK**
V2-n	18	3x5	[9,10,11]	**➔ scatter=1.52 <threshold=2 ➔ geometry OK**
V2-n	27	0	[10]	**➔ scatter=1.57 <threshold=2 ➔ geometry OK**
V2-n	27	1x3	[10]	**➔ scatter=1.42 <threshold=2 ➔ geometry OK**
V2-n	27	1x7	[10]	**➔ scatter=1.40 <threshold=2 ➔ geometry OK**
V2-n	27	1x10	[10]	**➔ scatter=1.52 <threshold=2 ➔ geometry OK**
V2-n	27	3x5	[3,10,14]	**➔ scatter=1.45 <threshold=2 ➔ geometry OK**
V2-n	27	3x5	[9,10,11]	**➔ scatter=1.57 <threshold=2 ➔ geometry OK**
V2-n	36	0	[0]	**➔ scatter=1.75 <threshold=2 ➔ geometry OK**
V2-n	36	1x3	[10]	**➔ scatter=1.56 <threshold=2 ➔ geometry OK**
V2-n	36	1x7	[10]	**➔ scatter=1.44 <threshold=2 ➔ geometry OK**
V2-n	36	1x10	[10]	**➔ scatter=1.78 <threshold=2 ➔ geometry OK**
V2-n	36	3x5	[3,10,14]	**➔ scatter=1.32 <threshold=2 ➔ geometry OK**
V2-n	36	3x5	[9,10,11]	**➔ scatter=1.55 <threshold=2 ➔ geometry OK**

measurement performance normalized wrt estimated installation costs

simulations run using: λ_{FIT}=0.7, mode relative amplitude A_0=0→1, σ=0.0→0.3, f_{maxM}=20→30, f_{maxS}=30→50;

1. **ITER-V3 geometry needs 36+3×5 sensors to satisfy requirements**
2. **optimized V2 geometry with 36 un-evenly spaced sensors is very resilient to the loss of sensors**
3. **adding too many high-resolution sensors does not necessarily improve the resilience of the measurement performance against the loss of sensors**

Resilience to Loss of Sensors: m-Results

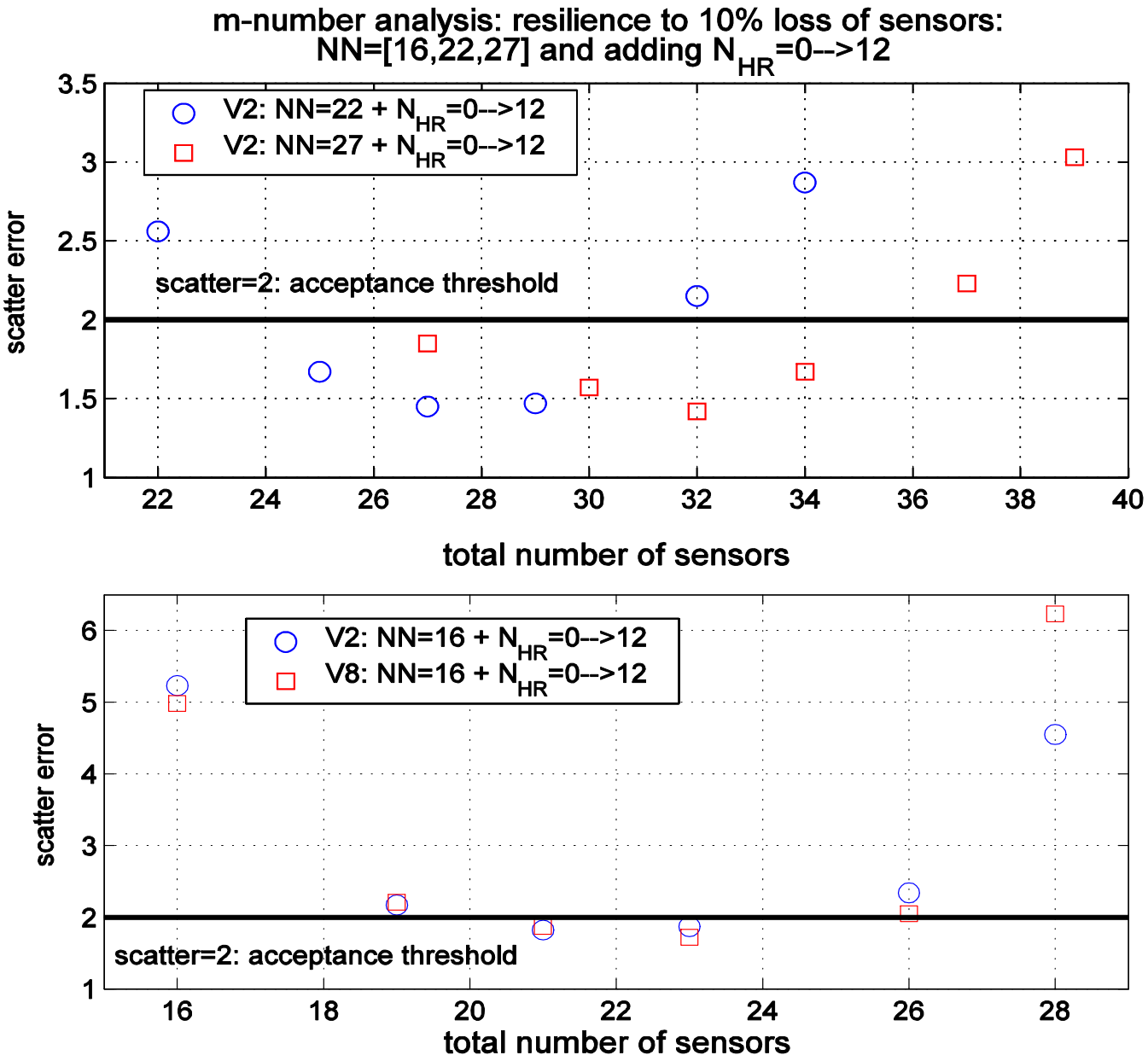

resilience of the optimized V2 and nominal V8 (ITER) geometries with NN=[16, 22, 27] sensors against a 10% failure rate for m-numbers analysis and always blacking-out the divertor region:

1. simulations run using λ_{FIT}=0.7, f_{maxM}=30→60, f_{maxS}=50→100, σ=0.0→0.3;
2. the original V8 geometry is sufficiently robust to satisfy the measurement requirements if one high resolution array with 5-7 sensors is added to its baseline implementation with 16 sensors
3. for NN=16, the V2 and V8 geometries perform equivalently
4. measurement performance of V2 geometry dramatically improves adding a few baseline sensors ➔ NN=22 better than NN=27!
5. the lowest scatter error as function of the number of high resolution sensors is always obtained when using 5-7 of them

measurement performance normalized wrt estimated installation costs

Resilience to Loss of Sensors: m-Results

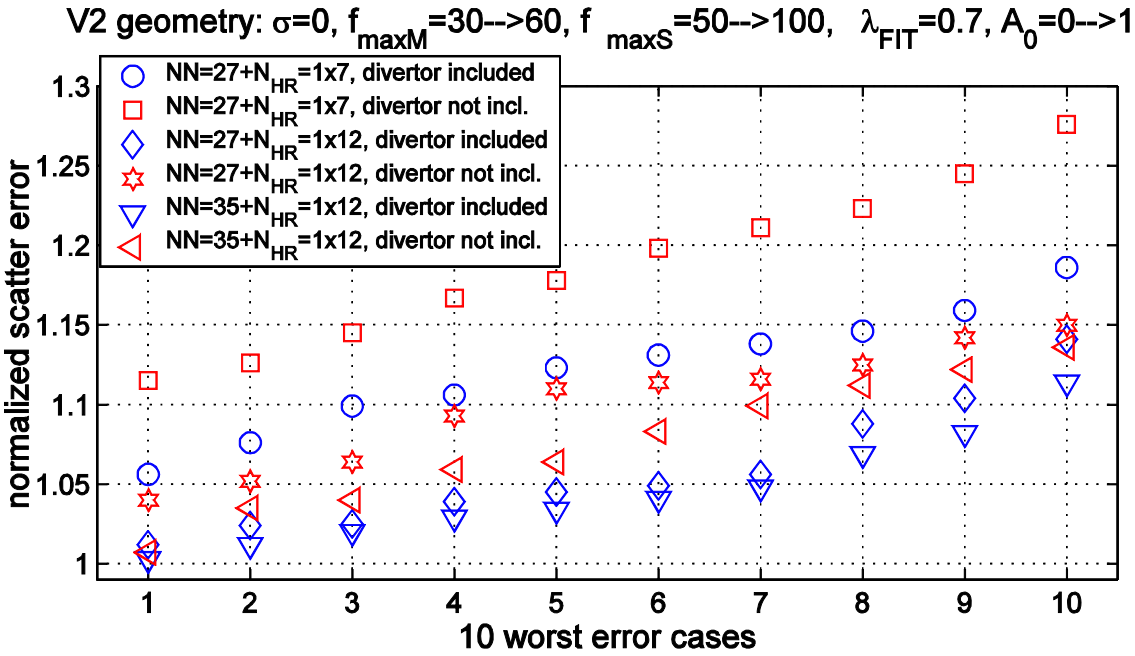

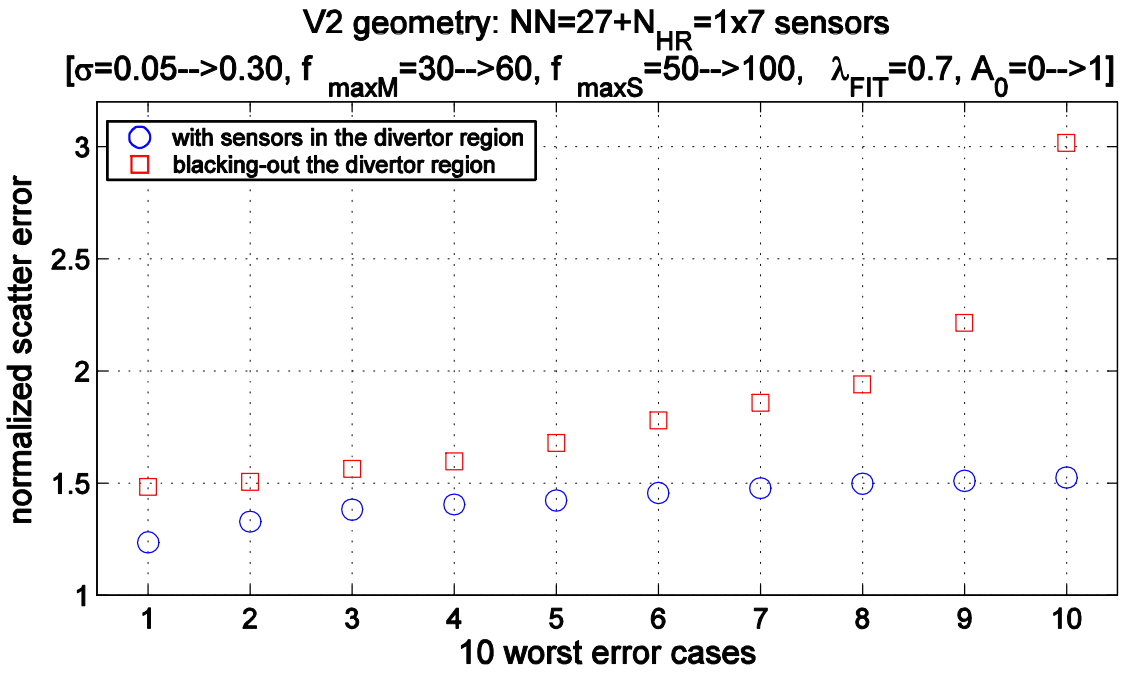

the 10 worst error cases for a nominal 10% loss of sensors for the V2 geometry for m-number analysis with/out blacking-out the divertor region and changing the number of baseline (NN) and high-resolution (N_{HR}) sensors;

1. simulations run using λ_{FIT}=0.7, mode relative amplitude A_0=0→1, f_{maxM}=30→60, f_{maxS}=50→100; σ=0→0.3;
2. when using a full coverage of the poloidal cross-section, the resilience against loss of sensors clearly improves;
3. if the input data are pure modes (σ=0), this improvement is less apparent;
4. for σ=0 there is a continuous improvement in the resilience against the loss of sensors for increasing number of sensors,
5. this improvement vs. the number of sensors does not occur so clearly for σ≠0

measurement performance normalized wrt estimated installation costs

Resilience to Loss of Sensors: m-Results

geometry	NN	NHR	NP	scatter in normalized fit error for a 10% failure rate
V8	16	0	[0]	➔ scatter=4.98, >threshold=2 ➔ geometry not ok
V8	16	1x3	[10]	➔ scatter=2.21, >threshold=2 ➔ geometry not ok
V8	16	1x7	[10]	**➔ scatter=1.72, <threshold=2 ➔ geometry OK**
V8	16	1x10	[10]	➔ scatter=2.05, >threshold=2 ➔ geometry not ok
V1-p	16	0	[0]	➔ scatter=145.56, >threshold=2 ➔ geometry not ok
V1-p	16	1x3	[10]	➔ scatter=87.52, >threshold=2 ➔ geometry not ok
V1-p	16	1x7	[10]	➔ scatter=5.66, >threshold=2 ➔ geometry not ok
V1-p	16	1x10	[10]	➔ scatter=10.34, >threshold=2 ➔ geometry not ok
V2-p	16	0	[0]	➔ scatter=5.23, >threshold=2 ➔ geometry not ok
V2-p	16	1x3	[10]	➔ scatter=2.17, >threshold=2 ➔ geometry not ok
V2-p	16	1x7	[10]	**➔ scatter=1.87, <threshold=2 ➔ geometry OK**
V2-p	16	1x10	[10]	➔ scatter=2.34, >threshold=2 ➔ geometry not ok
V2-p	22	0	[0]	➔ scatter=2.56 >threshold=2 ➔ geometry not ok
V2-p	22	1x3	[10]	**➔ scatter=1.67 <threshold=2 ➔ geometry OK**
V2-p	22	1x7	[10]	**➔ scatter=1.47 <threshold=2 ➔ geometry OK**
V2-p	22	1x10	[10]	➔ scatter=2.15 >threshold=2 ➔ geometry not ok
V2-p	27	0	[0]	**➔ scatter=1.85 <threshold=2 ➔ geometry OK**
V2-p	27	1x3	[10]	**➔ scatter=1.57 <threshold=2 ➔ geometry OK**
V2-p	27	1x7	[10]	**➔ scatter=1.67 <threshold=2 ➔ geometry OK**
V2-p	27	1x10	[10]	➔ scatter=2.23 >threshold=2 ➔ geometry not ok
V2-p	32	0	[0]	➔ scatter=2.07 >threshold=2 ➔ geometry not ok
V2-p	32	1x3	[10]	➔ scatter=2.02 >threshold=2 ➔ geometry not ok
V2-p	32	1x7	[10]	➔ scatter=2.12 >threshold=2 ➔ geometry not ok
V2-p	32	1x10	[10]	➔ scatter=3.86 >threshold=2 ➔ geometry not ok

simulations run using: λ_{FIT}=0.7, mode relative amplitude A_0=0→1, σ=0.0→0.3, f_{maxM}=30→60, f_{maxS}=50→100;

1. **ITER-V8 geometry needs 16+1×7 sensors to satisfy requirements**
2. **optimized V2 geometry with 27+1×3 un-evenly spaced sensors is the more resilient to the loss of sensors**
3. **adding too many high-resolution sensors does not necessarily improve the resilience of the measurement performance against the loss of sensors**

measurement performance normalized wrt estimated installation costs

Resilience to Loss of Sensors: Summary Conclusions

1. geometries with un-evenly spaced sensors are the more resilient against the loss of sensors
   - ➔ these geometries also allow for a major reduction in the total number of sensors in each individual array (with respect to geometries with periodicities in the sensors' positions)
   - ➔ for these geometries, adding further sensors does not necessarily improve the measurement performance once the reference spatial coverage is sufficient as the effect of random phase shifts due to the background noise starts to mask the "true" phase shifts due to the reduced spatial separation between the sensors
2. geometries made up of equi-spaced (sub-)assemblies present the lowest resilience to the loss of sensors, even if the initial total number of sensors is larger than that needed to obtain the required spatial Nyquist number
   - ➔ this can only be improved by breaking the original symmetries in the spatial sampling by adding high-resolution array(s) in port(s) separated as much as possible, with each additional array being made up of a small number (5-7) of un-evenly spaced sensors
   - ➔ however, this increases considerably the total number of sensors and associated in-vessel services that need to be installed

Optimization of the Sensors' Spacing and Spectral Window: Purpose

- background: the position of each individual sensor is not "absolutely" fixed, but there is a slightly larger volume where the sensor has to be located
  - calibration errors and uncertainties in the equilibrium reconstruction translate into an equivalent error on the nominal position of each sensor of up to ±3deg, when compared to the installation drawings and/or photogrammetry surveys
  - an improvement in the measurement performance achieved by displacing (some of) the sensors within this ±3deg tolerance, would correspond in practice to no changes being required for the installation drawings for the HF magnetic diagnostic system
  - if an improvement in modes number detection requires moving any of the HF magnetic sensors from a nominal geometry by more than the ±3deg nominal tolerance, this would then cause changes in the installation drawings for the HF magnetic diagnostic system
- **purpose of these tests**: change the sensors' position so as to further reduce the maxima of the spectral window for integer mode numbers
- **outcome of these tests**: identify the more robust sensor configurations vs. installation, calibration and data analysis inaccuracies

  ➔ the more the sensors need to be displaced to optimize the measurement performance against variations in the input mode spectrum modes, the less robust is this geometry

Optimization of the Sensors' Spacing and Spectral Window: n-Results

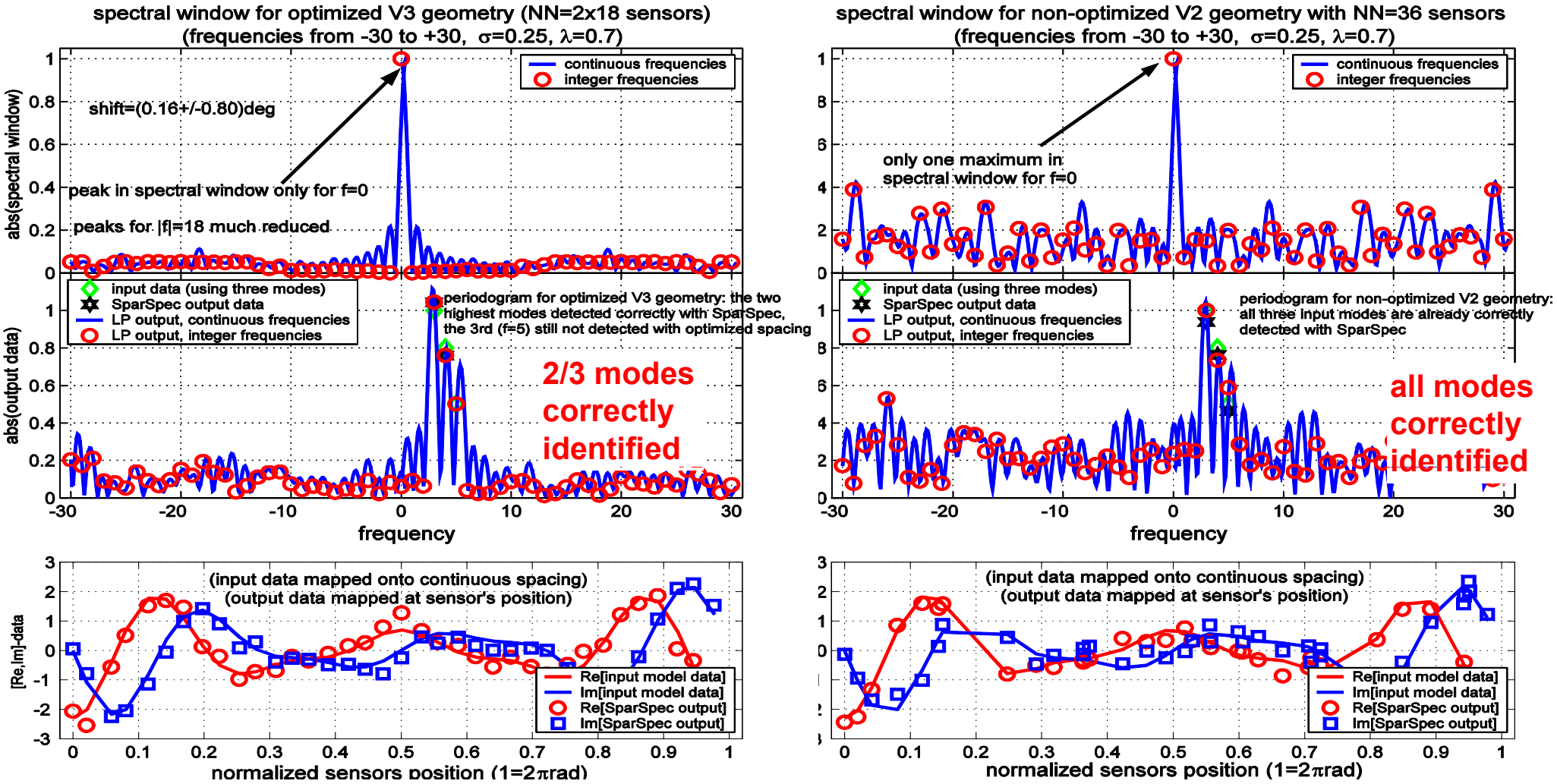

1. spectral window for the "optimized" ITER-V3 and the non-optimized V2 geometry, using 3 input modes
2. allowing ±5deg shift in the sensors' position to optimize measurement performance (cost-normalized)
3. **just the top two modes A_0>0.7 are detected using the "optimized" ITER-V3 geometry**
4. **all modes with A_0>0.3 are already detected with the non-optimized V2 spacing**

Optimization of the Sensors' Spacing and Spectral Window: n-Results

- adding some high-resolution sensors can really be beneficial for improving the measurement performance
- but adding too many of such sensors has a negative effect on the measurement performance
- this happens because the background noise starts to dominate over the measured signal for the sensors which are too closely spaced

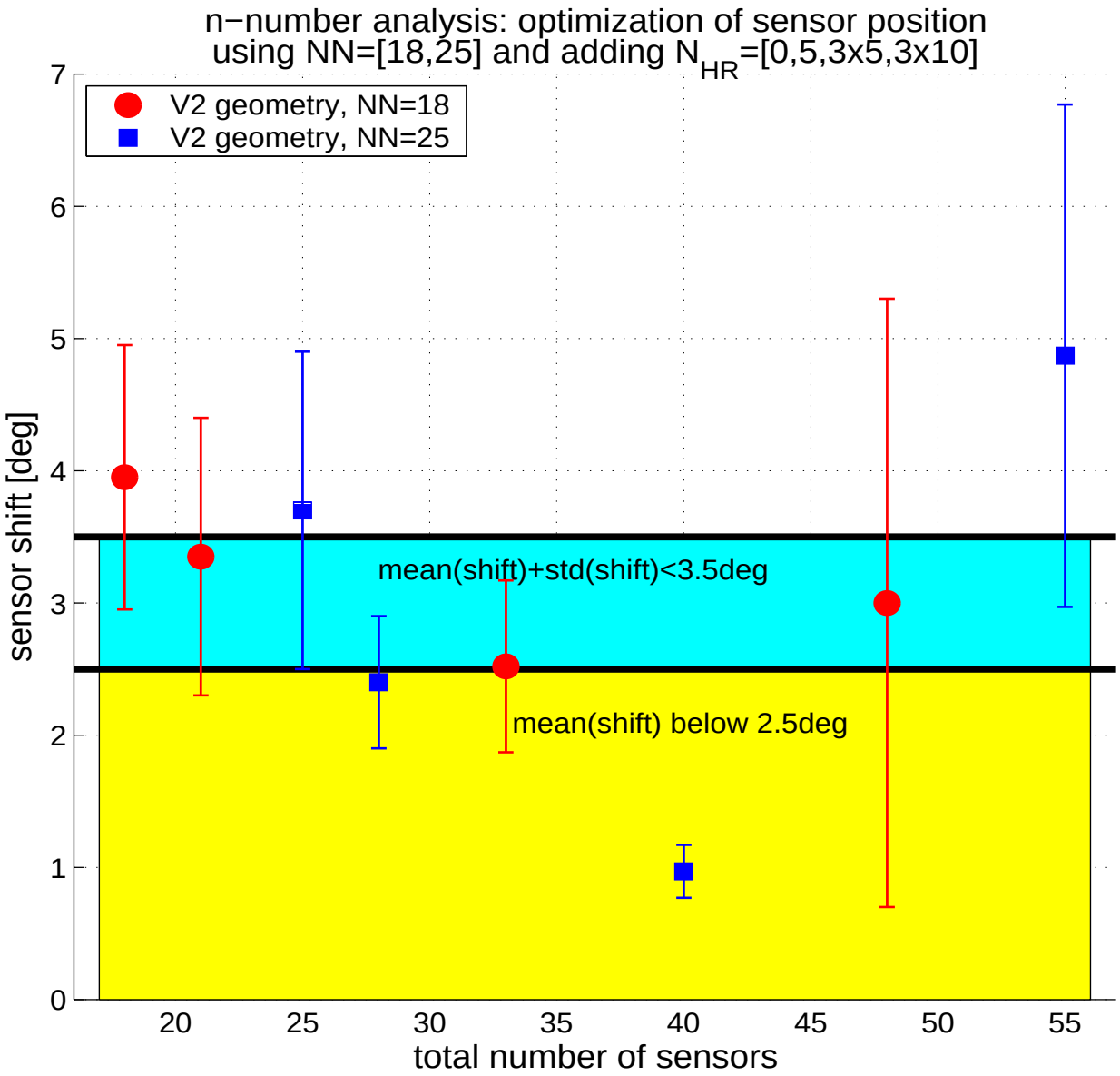

Optimization of the Sensors' Spacing and Spectral Window: m-Results

- adding some high-resolution sensors can really be beneficial for improving the measurement performance
- but adding too many of such sensors has a negative effect on the measurement performance
- the measurement performance of the V2 baseline geometry can be optimized more easily than the V8 geometry as it requires on average a smaller displacement of the sensors

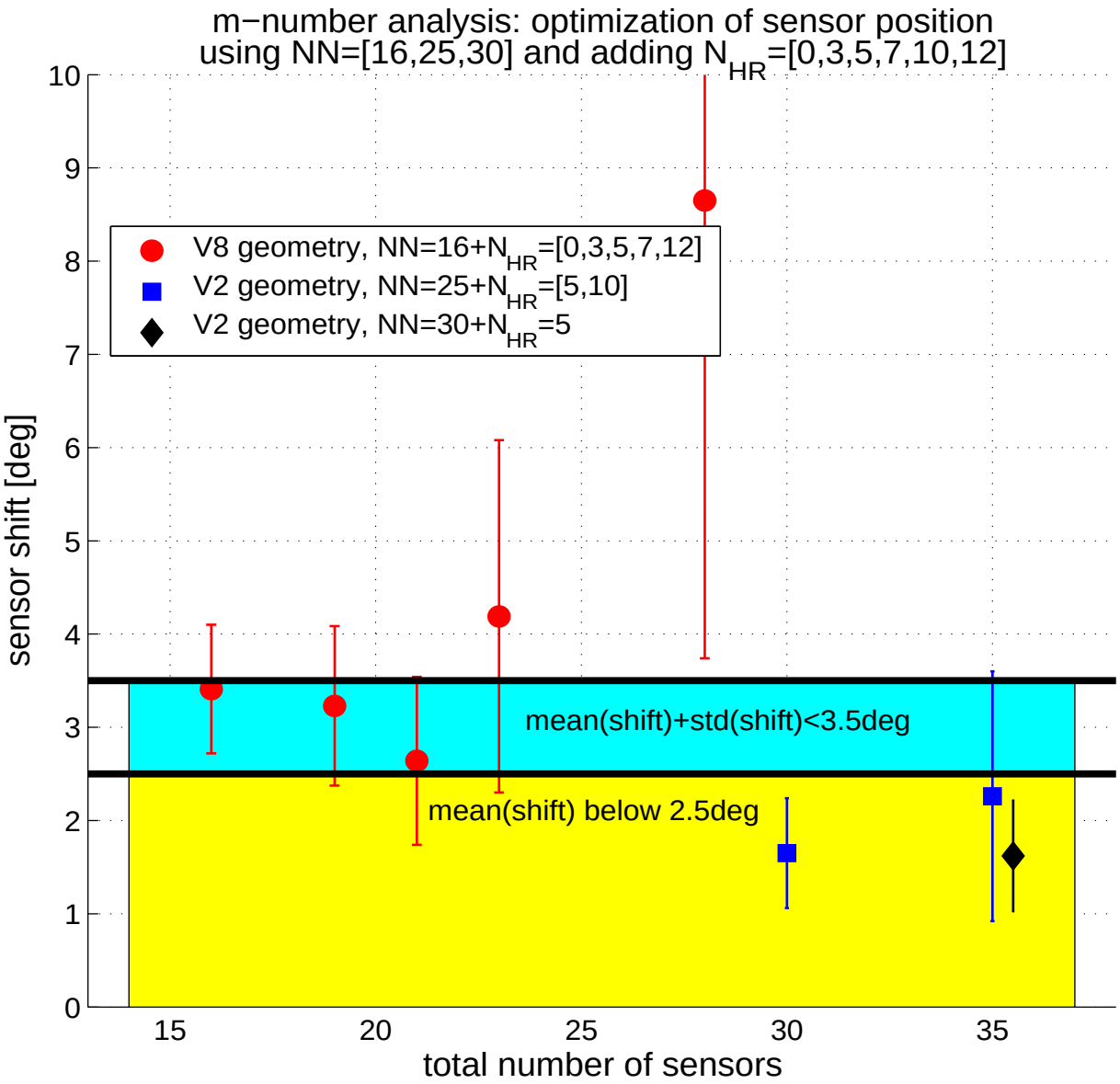

Optimization of the Sensors Spacing and Spectral Window: Summary Conclusions

1. sensor arrangements which are made up of equi-spaced sub-assemblies are those for which the sensors' displacement needed to improve the measurement performance is larger, with the effect on the modes' detection being the smaller
2. too closely spaced sensors are always significantly relocated so that, effectively, their separation is such that a "true" phase shift due to the input spectrum can be distinguished from the one due to white background noise
3. increasing the total number of both baseline and high-resolution sensors does not necessarily make their location less subject to optimization

Summary of Results on Optimization of ITER System Design for HF Magnetic Sensors (1)

- **the analysis of the baseline system design demonstrates that the nominal implementation of the magnetic sensors for MHD analysis does not satisfy the measurement requirements for toroidal and poloidal mode number analysis in ITER**
  - **analysis performed using normalization of measurement performance wrt to estimated R&D and installation costs**
  - toroidal mode number analysis: spatial symmetries in sensor geometry giving intrinsic Nyquist number: n=18 for noise variance σ=0
  - poloidal mode numbers: not enough sensors, non-optimized spatial coverage, large regions blacked-out
- **design optimized geometry for ITER magnetic sensors for MHD analysis by minimizing the maximum of spectral window for integer frequencies**
  - coherently with algorithm of Sparse Representation of signals
  - analysis done, optimized “ideal” geometry has been determined

Summary of Results on Optimization of ITER System Design for HF Magnetic Sensors (2)

- sensor arrangements made of sub-assemblies with spatial periodicities are more prone to fault detection of high-n(m) modes
  - this situation is only marginally improved by adding high-resolution array(s) inside the equatorial port(s)
- un-evenly spaced sensors arrangements are the more robust against false detection of high-n(m) modes if the spatial coverage is sufficiently complete
  - adding high-resolution array(s) inside equatorial port(s) does not improve significantly the system performance
- if the spatial coverage leaves significantly large regions blacked-out, adding a small number of sensors in high-resolution arrays inside the equatorial ports does improve the resilience against false detection of high-n(m) modes
- the best use of high resolution arrays inside equatorial ports is to have a relatively low number of sensors (5 to 7) in ports as far apart as possible

Risk Management for the ITER HF Magnetic Diagnostic System

- **integrate the physics requirements for the HF magnetic diagnostic system with the guidelines given in the ITER risk management plan:**

1. **redundancy** in the number of sensors in each individual measurement array, which we can take to be of the order of 20%, so as to mitigate the risk of "statistical" failure of any number of individual sensors
2. **multiplication** of such array at various positions using different geometries so as to mitigate the risk of common mode failure of an entire measurement array because of environmental conditions (localized radiation, nuclear and thermal damage, …) or "unknown plasma operation and physics unknowns" at the time of in-vessel installation that may render one geometry less capable of achieving the intended measurement performance at a later date
    - an example of such "unknown unknowns" not currently being dealt with is the possibility of plasmas at least partially limited on the high-field side wall: as no arrays for the measurement of toroidal mode numbers are currently foreseen at these locations, the MHD analysis of such plasmas would be very detrimentally affected

Optimized Layout for the ITER HF Magnetic Diagnostic System

1. toroidal mode number analysis: on the low field side, 2 arrays at the Z-height of each horizontal side of the equatorial port, each array made of 20-25 un-evenly spaced sensors plus 6x5 high resolution arrays located in each one of the equatorial ports used by the poloidal HF magnetic sensor system
   ➔ *this will provide redundancy in the n-number analysis against statistical loss of individual sensors using two largely over-sized measurement arrays*
2. toroidal mode number analysis: on both the low- and high-field sides, 2 further arrays of 25-35 un-evenly spaced sensors located approximately between 45cm and 70cm above and below the Z-centre of each equatorial port
   ➔ *this will provide redundancy in the n-number analysis against common mode failure of sensors due to environmental conditions and flexibility in the detection capabilities*
3. poloidal mode number analysis: one array of 20-35 un-evenly spaced plus 5-7 high resolution sensors replicated in six non equi-distant machine sectors (for instance using the equatorial ports NP=[1, 3, 8, 10, 14, 17], not covering the divertor region
   ➔ *this will provide redundancy in the m-number analysis against statistical loss of individual sensors using over-sized measurement arrays and against common mode failures and unknown unknowns as different vessel positions are used*

- **optimization performed taking into account normalization of measurement performance wrt to estimated R&D and installation costs**
- **very large redundancy in the measurement of HF magnetic instabilities**
- **using at least 2x(20-25+30) (a) + 4x(25-35) (b) + 6x(25-35+5-7) (c) = 350-500 sensors for measurement and analysis of high-frequency MHD instabilities in ITER**
  - *this is at least twice the original number of approximately 170 HF sensors*

Toroidal Mode Number Analysis: Optimized Layout, Spectral Window

- spectral window and spatial configuration of the “best” sensors geometries for toroidal mode number analysis (**cost-optimized**):

(a) non-optimized V3, 2x18 sensors

(b) partially optimized V3b, using 2x18+3x5 high-resolution sensors in the equatorial ports [3,10,14]

(c) fully optimized V2a for low-field side measurement at the Z-height of the corners of the equatorial port, using 25+3x5 high-resolution sensors in the equatorial ports [3,10,14]

(d) fully optimized V2b for high-field side and low-field side measurement at Z other than the corners of the equatorial port, using 30 baseline sensors

- all optimized geometries have a rather flat spectral window, with no local maxima other than for n=0

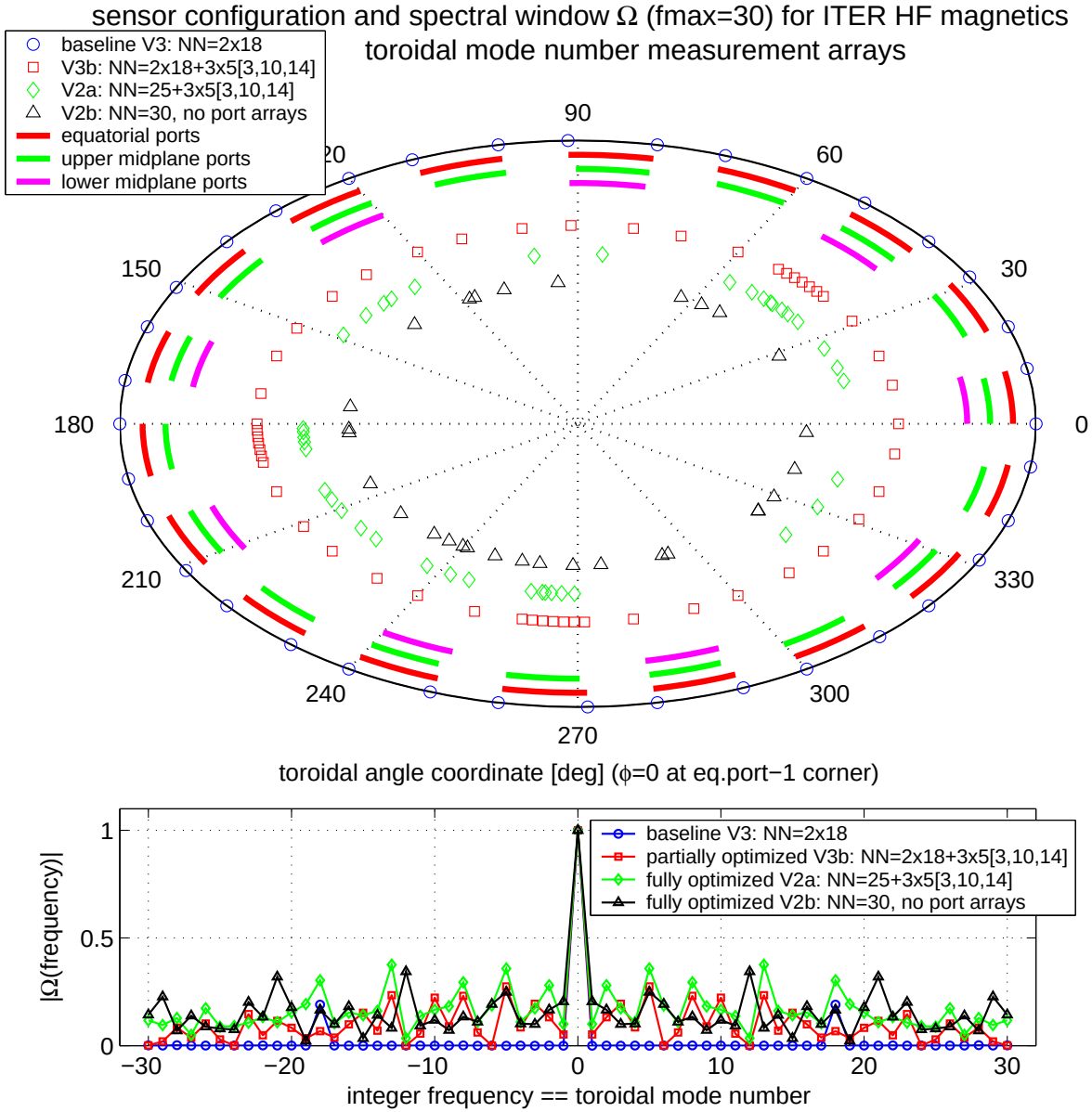

Poloidal Mode Number Analysis: Optimized Layout, Spectral Window

- spectral window and spatial configuration of the “best” sensors geometries for poloidal mode number analysis (**cost-optimized**):

(a) non-optimized V8, with16 sensors

(b) partially optimized V8b, using 16+1x7 high-resolution sensors

(c) fully optimized V2a, using 25+1x7 high-resolution sensors, not considering poloidal angles 75<|θ|(deg)<105

(d) fully optimized V2b, using 30+1x7 high-resolution sensors, now considering poloidal angles 75<|θ|(deg)<105

- the nominal V8 geometry has on the average higher values of the spectral window for integer poloidal mode numbers, but in all cases there are no clear local maxima other than for m=0

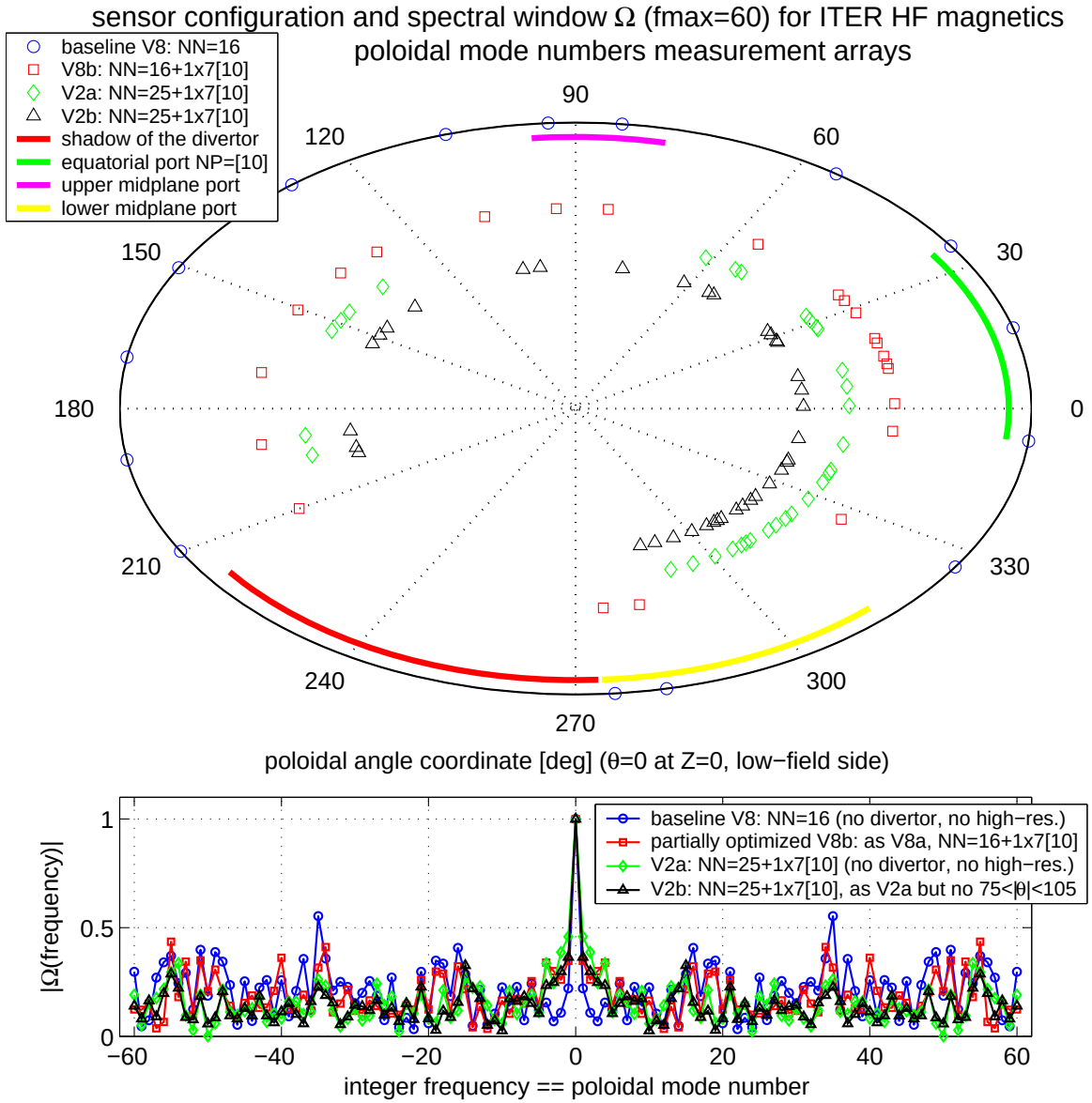

CONCLUSIONS

- status of system design
  - original system design for HF magnetic diagnostic system does not meet current ITER requirements for the measurement performance
  - optimized solution has been found on the basis of cost-normalized physics requirements, but using ~350-500 sensors instead of ~170
  - need to fully integrate in-vessel constraints to finalize system design
- status of HF sensor's prototyping (see poster by M.Toussaint):
  - current ITER design for Mirnov-type coil not OK
  - 1D and 3D HF magnetic sensors using the LTCC technology being developed as alternative concept
- **all these R&D and prototyping studies need to be completed by mid-2011 to meet current timeline for diagnostic implementation on ITER**